THE JOURNAL OF COMPARATIVE NEUROLOGY 496:314–334 (2006)

Unique Combination of Anatomy and Physiology in Cells of the Rat Paralaminar Thalamic Nuclei Adjacent to the Medial Geniculate Body

PHILIP H. SMITH,[1]* EDWARD L. BARTLETT,[2] AND ANNA KOWALKOWSKI[1]
[1]Department of Anatomy, University of Wisconsin, Medical School—Madison, Madison, Wisconsin 53706
[2]Department of Biomedical Engineering, Johns Hopkins University, Baltimore, Maryland 21205

ABSTRACT

The medial geniculate body (MGB) has three major subdivisions, ventral (MGV), dorsal (MGD), and medial (MGM). MGM is linked with paralaminar nuclei that are situated medial and ventral to MGV/MGD. Paralaminar nuclei have unique inputs and outputs compared with MGV and MGD and have been linked to circuitry underlying some important functional roles. We recorded intracellularly from cells in the paralaminar nuclei in vitro. We found that they possess an unusual combination of anatomical and physiological features compared with those reported for "standard" thalamic neurons seen in the MGV/MGD and elsewhere in the thalamus. Compared with MGV/MGD neurons, anatomically, 1) paralaminar cell dendrites can be long, branch sparingly, and encompass a much larger area; 2) their dendrites may be smooth but can have well defined spines; and 3) their axons can have collaterals that branch locally within the same or nearby paralaminar nuclei. When compared with MGV/MGD neurons, physiologically, 1) their spikes are larger in amplitude and can be shorter in duration; 2) their spikes can have dual afterhyperpolarizations with fast and slow components; and 3) they can have a reduction or complete absence of the low-threshold, voltage-sensitive calcium conductance that reduces or eliminates the voltage-dependent burst response. We also recorded from cells in the parafascicular nucleus, a nucleus of the posterior intralaminar nuclear group, because they have unusual anatomical features that are similar to those of some of our paralaminar cells. As with the labeled paralaminar cells, parafascicular cells had physiological features distinguishing them from typical thalamic neurons. J. Comp. Neurol. 496:314–334, 2006.

Indexing terms: calcium burst; intralaminar nuclei; parafascicular nucleus

Since the early brain-slice work of Jahnsen and Llinas (1984a,b), studies have shown that thalamocortical (TC) cells function in two different response modes, "burst" and "tonic," that depend on the activation of a low-threshold, voltage-sensitive calcium (Ca) conductance, which generates a transient current known as I_T. At a membrane potential of about –70 mV, synaptic inputs to TC cells activate the Ca conductance, resulting in a large, rapid depolarization that can elicit three to five high-frequency (>200 Hz) spikes with variable first-spike timing. If depolarized to –50 or –60 mV, the Ca conductance is inactivated, and the same synaptic input will instead elicit a shorter latency, well-timed spike. Thus, a TC cell's firing mode alters its spike response to ascending synaptic messages (see Sherman, 2001) and subsequently the temporal information being sent to cortex.

Reports of recordings from cells in the auditory thalamus or medial geniculate body (MGB; Hu, 1995; Peruzzi et

Grant sponsor: National Institutes of Health; Grant number: R01 DC006212 (to P.H.S.).

*Correspondence to: Philip H. Smith, Department of Anatomy, University of Wisconsin, 1300 University Avenue, Madison, WI 53706. E-mail: smith@physiology.wisc.edu

Received 4 August 2005; Revised 30 September 2005; Accepted 22 November 2005

DOI 10.1002/cne.20913

Published online in Wiley InterScience (www.interscience.wiley.com).

al., 1997; Tennigkeit et al., 1997; Bartlett and Smith, 1999) confirmed that virtually all TC cells in the two main MGB subdivisions, the dorsal and ventral MGB (MGD and MGV), show membrane potential dependent burst and tonic modes. MGV and MGD are the two primary areas of the auditory thalamus. MGV is part of the tonotopically organized primary or "lemniscal" pathway, whereas MGD is a component of the "extra- or nonlemniscal" division (Clerici and Coleman, 1990; Clerici et al., 1990; Winer et al., 1999). In rats, almost all neurons in these regions are thalamocortical, projecting to intermediate layers of the auditory cortex (Roger and Arnault, 1989; Arnault and Roger, 1990; Clerici and Coleman, 1990; McMullen and de Venecia, 1993; Khazaria and Weinberg, 1994; Winer et al., 1999). In MGV, the TC cells have been called *tufted* or *bushy* based on highly intertwined dendritic trees. MGD is less homogeneous, but many TC cells here are classified as either tufted or stellate.

A third subdivision of the auditory thalamic complex, the medial division (MGM), has been described. MGM is one of a group of nuclei referred to as *paralaminar* (Herkenham, 1980) situated medial and ventromedial to the MGB. This group also includes the posterior interlaminar (PIN), suprageniculate (SG), and peripeduncular (PP) nuclei (Winer and Morest, 1983; LeDoux et al., 1987; Winer and Larue, 1988). Several unique features have been described regarding these areas. First, anatomical studies showed that, compared with MGV and MGD, cells here have the least uniformity of soma size (Morest, 1964; Clerici and Coleman, 1990; Clerici et al., 1990; Winer et al., 1999). Some dendritic trees may have tufted or stellate morphology, like MGV and MGD cells, but many others can show long, sparsely branching dendrites. Second, the inputs to these areas are multimodal, arriving not only from the inferior colliculus (IC) but from visual, somatosensory, and other centers as well (LeDoux et al., 1984, 1987; Peschanski, 1984; Hicks et al., 1986; Arnault and Roger, 1987; Bordi and LeDoux, 1994a,b; Benedek et al., 1997; Linke et al., 1999). Third, the outputs of cells here are diverse. As with MGV and MGD neurons, some cells in MGM and the other paralaminar nuclei are thalamocortical (Scheel, 1988; Roger and Arnault, 1989; Arnault and Roger, 1990; Clerici and Coleman, 1990; Brett et al., 1994; Linke, 1999; Winer et al., 1999; Doron and LeDoux, 2000), but, unlike MGV and MGD cells, they often project to layer 1 (Niimi and Matsuoka, 1979; Mitani et al., 1984, 1987; Linke and Schwegler, 2000; Kimura et al., 2003). Jones (1998a,b) speculated that this layer 1 projection may engage multiple cortical areas at times when it is necessary to "bind" the many aspects of a sensory experience together. This projection has also been implicated in the modulation of the cortical high-frequency 40-Hz gamma oscillations (Barth and McDonald, 1996; Sukov and Barth, 2001) and the expression of long-term cortical plasticity (Weinberger et al., 1995; Weinberger, 1998). Another major projection of paralaminar cells is to the amygdala. Work from LeDoux and others has shown this connection to be a vital part of the pathway responsible for the behavioral and autonomic responses elicited by the conditioned fear response (see, e.g., LeDoux et al., 1986, 1988; LeDoux, 1995; LeDoux and Muller, 1997; Linke et al., 2000, 2004). Paralaminar cells can also project to the basal ganglia (Moriizumi and Hattori, 1992; Shammah-Lagnodo et al., 1996; LeDoux et al., 1985) and the inferior colliculus (Senatorov and Hu, 2002; Winer et al., 2002).

Despite the participation of cells in the MGM and other paralaminar nuclei in the important functions listed above and their unusual inputs and outputs, no one has taken advantage of the slice preparation to compare their physiological properties with those of their "standard" TC counterparts. We have made sharp electrode recordings from MGM cells and cells of the adjacent paralaminar nuclei by using thalamic slices. We found that in vitro data from cells here reveal several unique and potentially important features that distinguish them from "standard" TC cells (see Sherman and Guillery, 2001).

MATERIALS AND METHODS

Intracellular recording

All methods were approved by the University of Wisconsin Institutional Animal Care and Use Committee. Animals were maintained in an American Associations for Accreditation of Laboratory Animal Care-approved facility. Our experimental methods are similar to those described previously (Peruzzi et al., 1997; Bartlett and Smith, 1999, 2002). Brain slices from 3–6-week-old Long-Evans hooded rats of either gender were used. Rats were given an anesthetic overdose then perfused transcardially with chilled, oxygenated sucrose saline (described below). The portion of the brain containing the thalamus was removed, and 500-μm horizontal or coronal slices were taken through the MGB. These two slice planes were used so that we could stimulate two major inputs to the MGM, the IC inputs in horizontal slices and the superior collicular (SC) inputs in coronal slices. Details of these synaptic inputs will be reported in a subsequent paper. Slices were placed in a submersion-style holding chamber containing oxygenated artificial cerebrospinal fluid (ACSF) at room temperature. After equilibration, one slice was transferred to the recording chamber and perfused with normal, oxygenated ACSF at 33–34°C, which contained the following (in mM): NaCl, 124; KCl, 5; KH_2PO_4, 1.2; $CaCl_2$, 2.4; $MgSO_4$, 1.3; $NaHCO_3$, 26; and glucose, 10. The sucrose ACSF contained sucrose instead of NaCl (Aghajanian and Rasmussen, 1989). For low-calcium saline, the calcium concentration was reduced from 2.4 mM to 0.4 mM. Nickel (Sigma-Aldrich Co., St. Louis, MO), 4-aminopyridine (4AP; Sigma-Aldrich Co.), and apamin (Vector, Burlingame, CA) were all mixed in ACSF at the stated concentrations on the day of the experiment and bath applied. Recording began at least 30 minutes after the slices were placed in the recording chamber.

Intracellular recordings of responses to injected current were made with glass microelectrodes of 100–150 MΩ resistance when filled with a solution of 2 M potassium acetate and 2% Neurobiotin (Vector). Cells were considered viable if their initial resting potential was more negative than –50 mV and their action potentials overshot 0 mV. Intracellular current and voltage records were digitized with a Digidata 1322A (Axon Instruments, Burlingame, CA) and saved in pClamp software for subsequent analysis.

Histology

During intracellular recording, Neurobiotin was injected into the recorded cell with a 0.3–0.5-nA current for 2–10 minutes. After the experiment, the slice was fixed in fresh 4% paraformaldehyde and cryoprotected, and 60–

70-μm frozen sections were cut and collected in 0.1 M phosphate buffer, pH 7.4. The sections were then incubated in H_2O_2, rinsed in phosphate buffer, then refrigerated and incubated overnight in the avidin-biotin-horseradish peroxidase (HRP) complex (ABC Kit; Vector). On the following day, the sections were rinsed in phosphate buffer, and the Neurobiotin was reacted with the diaminobenzidine (DAB)-nickel/cobalt intensification method, mounted, counterstained with cresyl violet, and coverslipped.

To determine a cell's location and make morphological measurements, camera lucida drawings were made. A low-power, ×40 drawing of the MGB and surrounding structures was made and the location of the labeled cell noted. The location of the cell body relative to the divisions of the rat MGB was determined by published reports of the differences in Nissl staining between MGM and SG (LeDoux et al., 1985) and by other landmarks in the vicinity that distinguish the location of PP and PIN. We also compared our sections/drawings with sections in the atlas of Paxinos and Watson (1986), illustrations in the cytoarchitectural study of Clerici and Coleman (1990), and the illustration of paralaminar subdivisions by LeDoux et al. (1985) and Doron and LeDoux (2000). A high-power, ×1,250 drawing of the cell body, dendritic tree, and initial portion of the axon was also made.

Data analysis, anatomy

Several measurements of the cell body and dendritic tree of our intracellularly labeled cells were made so that they could be compared with similar data from tufted and stellate cells in the MGV and MGD that we previously reported (Bartlett and Smith, 1999). The measurements described here were taken from the high-power drawing of the cell. Measurements were made only from cells where it was apparent that the majority of the dendrites were intact as indicated by the fact that they did not end abruptly at the top or bottom of the slice. Cell body areas were determined by drawing the outline of the cell body in Neurolucida software (MicroBrightField, Colchester, VT). Dendritic tree area was determined in the same software by drawing a line between the ends of adjacent dendrites and measuring the enclosed area. Another measure of the extent of the dendritic tree was dendritic projection distance, for which we measured and averaged the length of a cell's three longest dendrites. As a measure of dendritic branching, we used scaled circles of 50 and 100 μm, centered on the cell body, and counted the number of dendrites extending beyond these distances. This value was termed the *number of dendritic intersections*.

Data analysis, physiology

Several variables of the basic cell physiology were measured in Clampfit software (Axon Instruments) so that the data could be compared with our previous data from cells in the MGV and MGD (Bartlett and Smith, 1999). Resting potential was measured as the difference between the voltage measured extracellularly and intracellularly during recording. Input resistance was measured from the maximal voltage deflection to a −0.1-nA current pulse. Spike amplitude was measured as the voltage difference between rest and spike peak. Spike threshold was measured as the least amount of positive current required to generate a spike. Spike duration was measured as the duration of the spike at half-amplitude. The amplitude of the low-threshold Ca conductance was measured by the area under the rebound burst that occurred when the cell was hyperpolarized and then returned to rest. The range of DC levels over which a burst occurred was measured by injecting depolarizing or hyperpolarizing current to move the membrane potential around rest and noting whether a −0.3-0.5-nA current pulse elicited a burst.

Statistical analysis was performed in Origin Pro7 (OriginLab, Northampton, MA) and Microscoft Excel (Microscoft Corp., Seattle, WA). Data are presented as mean ± SD. A P value of ≤0.05 was considered to represent a significant difference.

RESULTS

We labeled 91 cells in 67 slices taken from 53 rats of either sex that were medial or ventral to the MGV/MGD in one of the adjacent paralaminar nuclei. No differences were noted in the basic anatomy or physiology of these cells between subdivisions, so they will be described as a single population. The terms *MGM* and *paralaminar* will be used interchangeably from this point onward.

Anatomy

Cell bodies. Clerici and Coleman (1990) and Winer et al. (1999) reported that rat MGM cell size is more diverse than MGV/MGD cell size, with the largest of MGM cell bodies classified as magnocellular. This was also the case with our intracellularly labeled population (Fig. 1). Paralaminar cell bodies showed a larger range of sizes (from 118 to 451 μm^2, mean 259 ± 81.5) than MGV/MGD cells (from 122 to 226 μm^2 mean 175 ± 35.8). In addition, one-way ANOVA indicated a significant difference among the means of MGM cell, MGV/MGD tufted cell, and MGD stellate cell sizes [$F(2,37) = 5.26$, $P = 0.01$]. Post hoc tests for differences in means showed that, although the mean for paralaminar cell size (259 ± 81.5 μm^2) was greater than that for stellate cells (182 ± 44.5 μm^2) and tufted cells (171 ± 33.1 μm^2), significance was reached only for the paralaminar/tufted cell difference (t-test, $P < 0.01$).

Dendritic trees. By using Golgi staining methods, Clerici and Coleman (1990) and Winer et al. (1999) reported on the dendritic tree configurations of rat MGM cells. Their sections were 100–150 μm thick, whereas our slices were 500 μm thick, so we were able to get a more complete picture of the tree configuration.

We noted significant differences in dendritic tree features of cells in the MGM and other paralaminar nuclei compared with those of tufted and stellate cells previously reported in MGV and MGD (Bartlett and Smith, 1999). For cells labeled in slices taken in either the horizontal or the coronal plane, some of our labeled paralaminar cells had multipolar or stellate dendritic configurations. For these cells, it was apparent that all or a large majority of the dendritic tree was present in the slice (Fig. 2). A number of the paralaminar cells labeled in coronal slices displayed elongated dendritic trees that extended for considerable distances primarily in the dorsoventral direction (Fig. 3). We saw cells labeled in our horizontal slices with several of their major dendrites cut off at the top and bottom of the slice and assume that these are probably the same elongate cells. Such cells from horizontal slices with incomplete dendritic trees were not included in the analysis. In the coronal plane, these cells with elongated, oriented trees had a small number of long, sparsely branch-

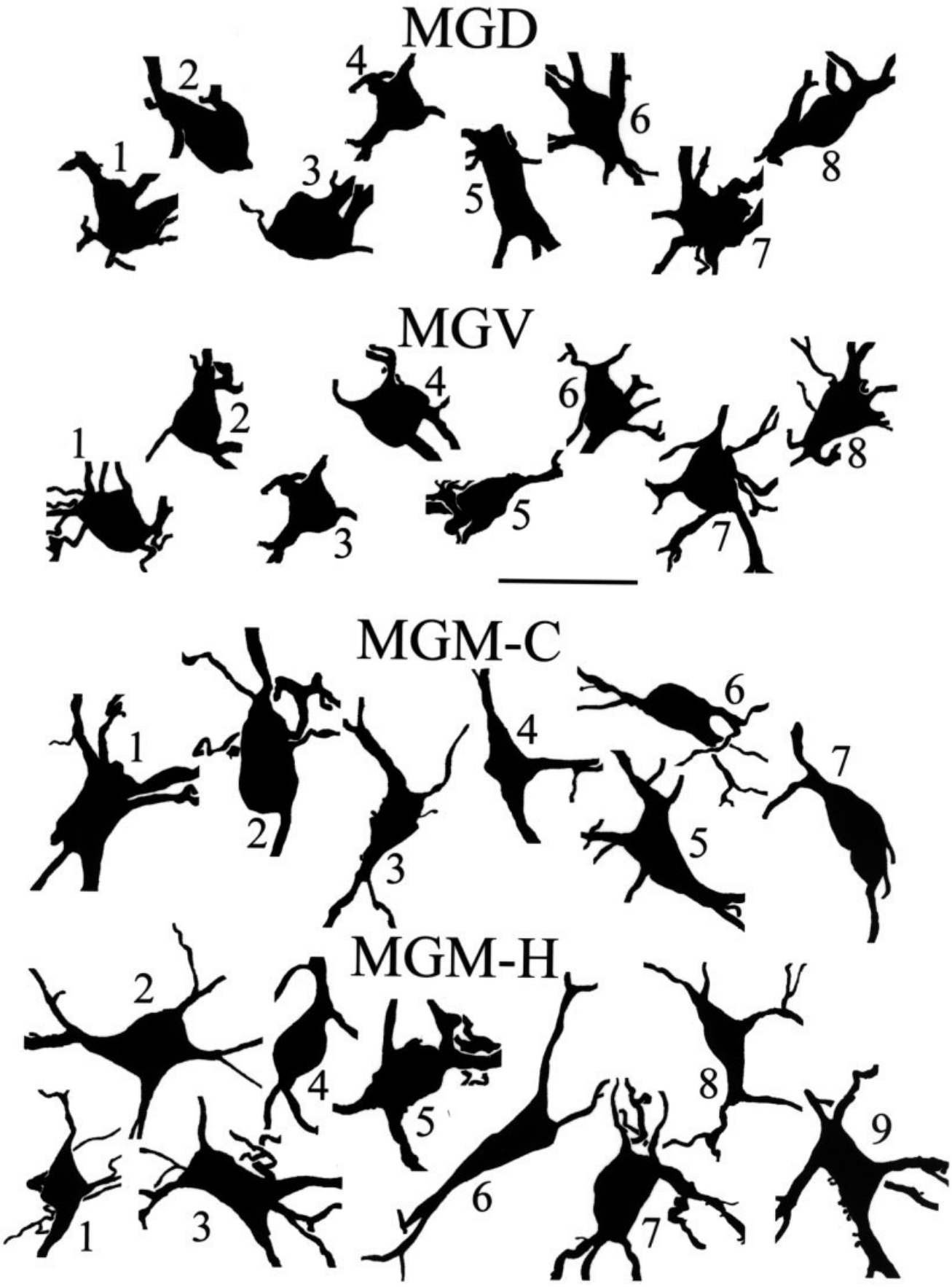

Fig. 1. Camera lucida drawings of the cell bodies and primary dendrites of tufted and stellate cells in the dorsal (MGD) and ventral (MGV) divisions of the MGB in comparison with similar drawings made of stellate and elongate cells in the intralaminar nuclei adjacent to the MGB that were labeled either in the coronal (MGM-C) or horizontal (MGM-H) plane. Scale bar = 50 μm (applies to all).

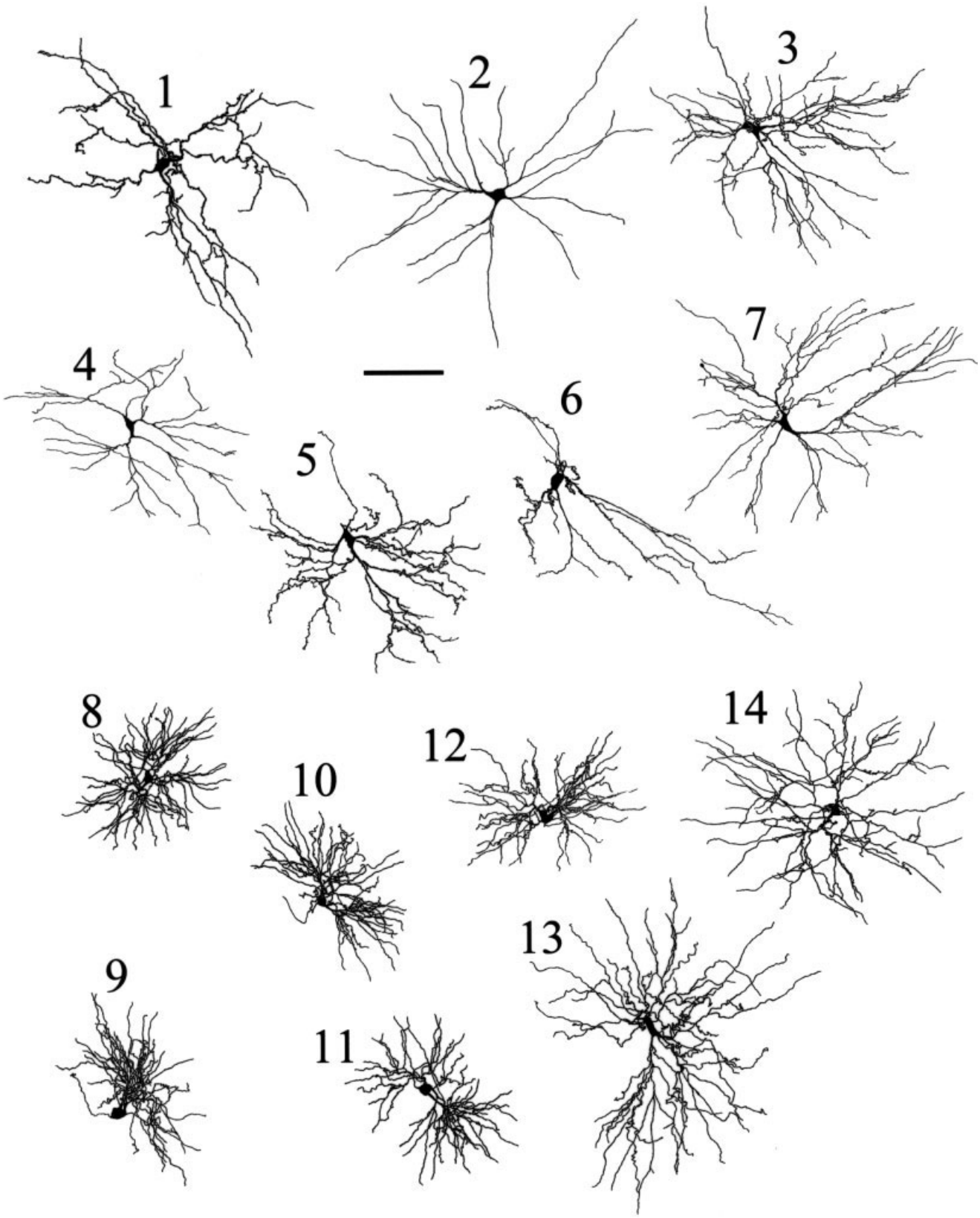

Fig. 2. Comparison of paralaminar multipolar/stellate cells with stellate and tufted cells of the MGV and MGD. 1–7: Camera lucida drawings of seven multipolar/stellate cells located in the medial division of the medial geniculate or other paralaminar nuclei adjacent to the medial geniculate. Cells 2 and 7 were labeled in the coronal plane, cells 1 and 3–6 in the horizontal plane. 8–12: Camera lucida drawings of five tufted neurons located in the ventral or dorsal divisions of the medial geniculate. 13,14: Camera lucida drawings of stellate cells located in the dorsal division of the medial geniculate. Scale bar = 100 μm (applies to all).

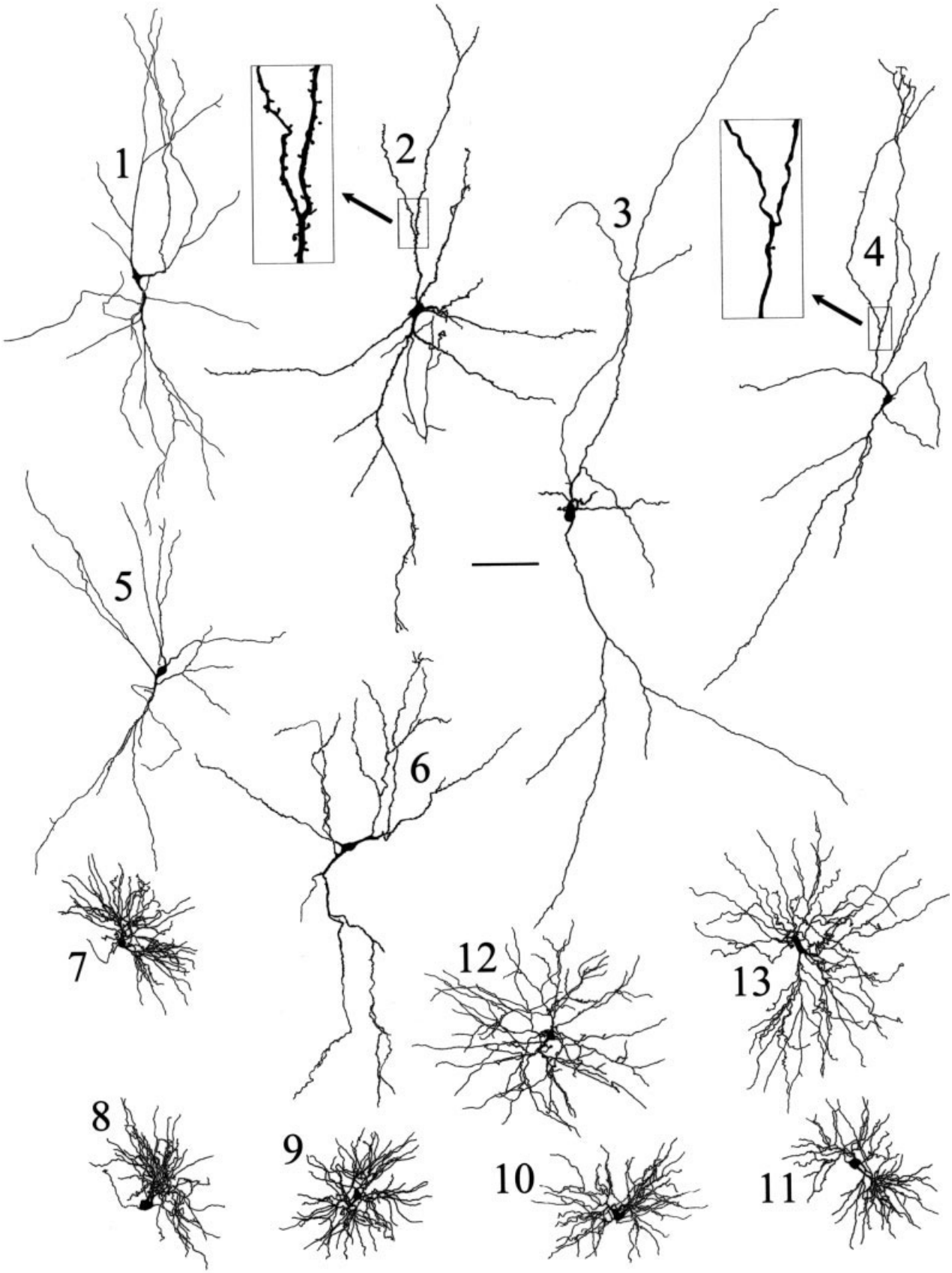

Fig. 3. Comparison of elongate cells in the paralaminar nuclei with stellate and tufted cells in the MGV and MGD. 1–6: Camera lucida drawings of examples of cells in the paralaminar nuclei labeled in the coronal plane exhibiting very long, sparsely branching dendritic trees, which could display numerous spines (cell 2 inset) or only an occasional spine or no spines (cell 4 inset). 7–13: Camera lucida drawings of tufted (7–11) or stellate (12,13) cells labeled in the ventral or dorsal divisions of MGB. These are the same MGB cells seen in Figure 2. Scale bar = 100 μm (applies to all).

ing dendrites that could extend for over 1 mm. The terminal branches often encroached on a paralaminar nucleus adjacent to the one containing the cell body (Figs. 4, 5). Despite their dorsoventral extent, dendrites of these cells usually did not venture far enough laterally to encroach significantly on the MGV or MGD. There was no clear correlation between soma size and the area of the dendritic arbor, except that the smallest MGM cells (areas less than 175 μm^2) had the smallest arbor areas, which were still larger than the MGV arbor areas. Thus, cell bodies that were intermediate in size (200–300 μm^2) and cell bodies that could be classified as magnocellular (soma areas greater than 300 μm^2) could have large, elongate dendritic trees with large areas but could also have multipolar/stellate dendritic trees with smaller areas.

As might be expected from their extensive dendritic lengths, the dendritic tree areas of these elongate cells were significantly larger than those of tufted or stellate cells of the MGV and MGD. A one-way ANOVA on the dendritic trees of MGM cells labeled in the coronal slices and stellate and tufted cell dendrites in the MGV and MGD showed significant differences in the means [$F(2,34) = 15.88$, $P < 0.0001$]. Post hoc *t*-tests for the differences in the means showed that the dendritic tree areas of MGM cells measured in this plane (122,260 ± 64,701 μm^2) were significantly larger than both the MGV/MGD tufted (area = 29,333 ± 5,777 μm^2, $P < 0.0001$) and MGD stellate (62,830 ± 12,723 μm^2, $P < 0.05$) dendritic trees. The larger examples of elongate dendritic trees could measure over four times greater than the average MGD stellate cell and over 8–10 times the average MGV/MGD tufted cells. Likewise, the length of the three longest MGM dendrites of these elongate cells in the coronal plane could be over 500 μm. The results of a one-way ANOVA showed significant differences among the means of the groups [$F(2,29) = 27.0$, $P < 0.0001$]. Post hoc *t*-tests revealed that the MGM cell dendrites in the coronal plane were significantly longer (372 ± 111 μm) than dendrites of either tufted cells in MGV/MGD (143 ± 19.2 μm, $P < 0.0001$) or stellate cells in MGD (204.7 ± 19.2 μm, $P < 0.002$).

One simple way in which we quantified and compared dendritic branching patterns between paralaminar and MGV/MGD neurons was to count the number of branches located at 50 μm or 100 μm radial to the cell body. One-way ANOVA showed a significant difference in the means when comparing these features for MGM cells, tufted cells in MGV/MGD, and stellate cells in MGD [at 50 μm, $F(2,32) = 87.8$, $P < 0.0001$; at 100 μm, $F(2,32) = 38.2$, $P < 0.0001$]. Post hoc analysis of the means revealed that the paralaminar elongate cells (as illustrated in Fig. 3) had significantly fewer branches at both 50 μm (8 ± 3.73) and 100 μm (10.9 ± 4.4) than either tufted cells (40.2 ± 9.2, $P < 0.0001$; 22.4 ± 7.9, $P < 0.001$) or stellate cells (29.7 ± 5.89, $P < 0.001$; 32.8 ± 5.4, $P < 0.001$) in MGV/MGD. ANOVA tests also revealed that the dendritic branching patterns of the stellate/multipolar population of MGM cells were significantly different from the patterns of their counterparts in the MGD at both 50 μm [$F(2,27) = 63.1$, $P < 0.0001$] and 100 μm [$F(2,27) = 19.7$, $P < 0.0001$]. Post hoc *t*-test analysis indicated that the MGM stellate/multipolar cells had significantly ($P < 0.0001$) fewer branches at 50 μm (8.75 ± 2.6) and 100 μm (12.9 ± 4.3) than their counterpart stellate cells in MGD (at 50 μm, 29.7 ± 5.89; at 100 μm, 32.8 ± 5.4). However, despite having fewer branches, the dendritic tree areas of the MGM stellate cells (59,808 ± 26,895 μm^2) did not differ significantly from those of the MGD stellate cells (62,830 ± 12,723 μm^2)

Another unique feature of some (20%) of the MGM/paralaminar cells was the presence of numerous dendritic spines along the length of the dendrite (Fig. 3, cell 2 inset; Fig. 4D). Although we (Bartlett and Smith, 1999) and others (Winer et al., 1999) have seen some dendritic specializations (knob-like bumps, short dendritic appendages, some spines) on MGV or MGD TC cells, those on MGM cells could be more numerous and more consistently resembled spines (a distinct spine head and shaft). These spiny dendrites could belong to either the multipolar/stellate or the elongate cell types. In contrast, the remainder of the stellate and elongate cells had dendritic trees with very few spines (Fig. 3, cell 4 inset). These cells were darkly labeled, so it was not simply a problem of being unable to visualize appendages.

Thus, the paralaminar cell bodies had a wider range of sizes and tended to be larger than tufted MGV/MGD cells. The dendritic trees of cells in paralaminar nuclei could be multipolar/stellate or could be elongate, extending for very long distances, primarily in the coronal plane. MGM elongate cell dendritic trees encompassed a significantly larger area than those of stellate cells in MGD or tufted cells in MGV/MGD. Stellate/multipolar cells in MGM had dendritic trees that were significantly larger than tufted MGV/MGD cells but not different from stellates in MGD. Both elongate and multipolar/stellate cell types in MGM tended to have fewer dendritic branches than the MGV and MGD cell types and could bear numerous dendritic spines. Cell body size was not a good predictor of dendritic size except that smaller cell bodies tended to have smaller dendritic trees. We labeled only a small number of cells in the paralaminar nuclei that might be considered tufted, and these were usually close to the borders between the paralaminar and the dorsal or ventral nuclei. They were not included in the analysis.

Axons. Another difference between TC cells in MGV and MGD and cells in adjacent paralaminar nuclei was the presence of local axon collaterals. In our previous study (Bartlett and Smith, 1999), none of the TC cells in MGV and MGD showed axon collaterals within or near the MGB. In contrast, some (10%) of our MGM cells displayed one or more collaterals (Figs. 4, 5) with en passant and en terminaux swellings (Figs 4C, arrows). This percentage is likely to be an underestimate, because these collaterals could arise several hundred micrometers down the main axon (Fig. 4A), and, in slice preparations, main axons are often cut off close to their origin on the cell body or dendritic tree. The collaterals typically arose from the axons of cells that also had spiny dendritic trees. They could branch and display swellings near the parent cell (Fig. 5) or could come off the main axon at more distant sites to innervate other paralaminar regions (Fig. 4). None of the collaterals was seen entering MGV or MGD.

Physiology

General. Stable intracellular recordings from cells in paralaminar nuclei could last for several hours, and resting membrane potentials (−65 ± 6.7 mV) were not significantly different from those of cells in MGV and MGD that we previously reported (−62.2 ± 8.8 mV). Action potential amplitudes of paralaminar cells (72.1 ± 10.9 mV) were

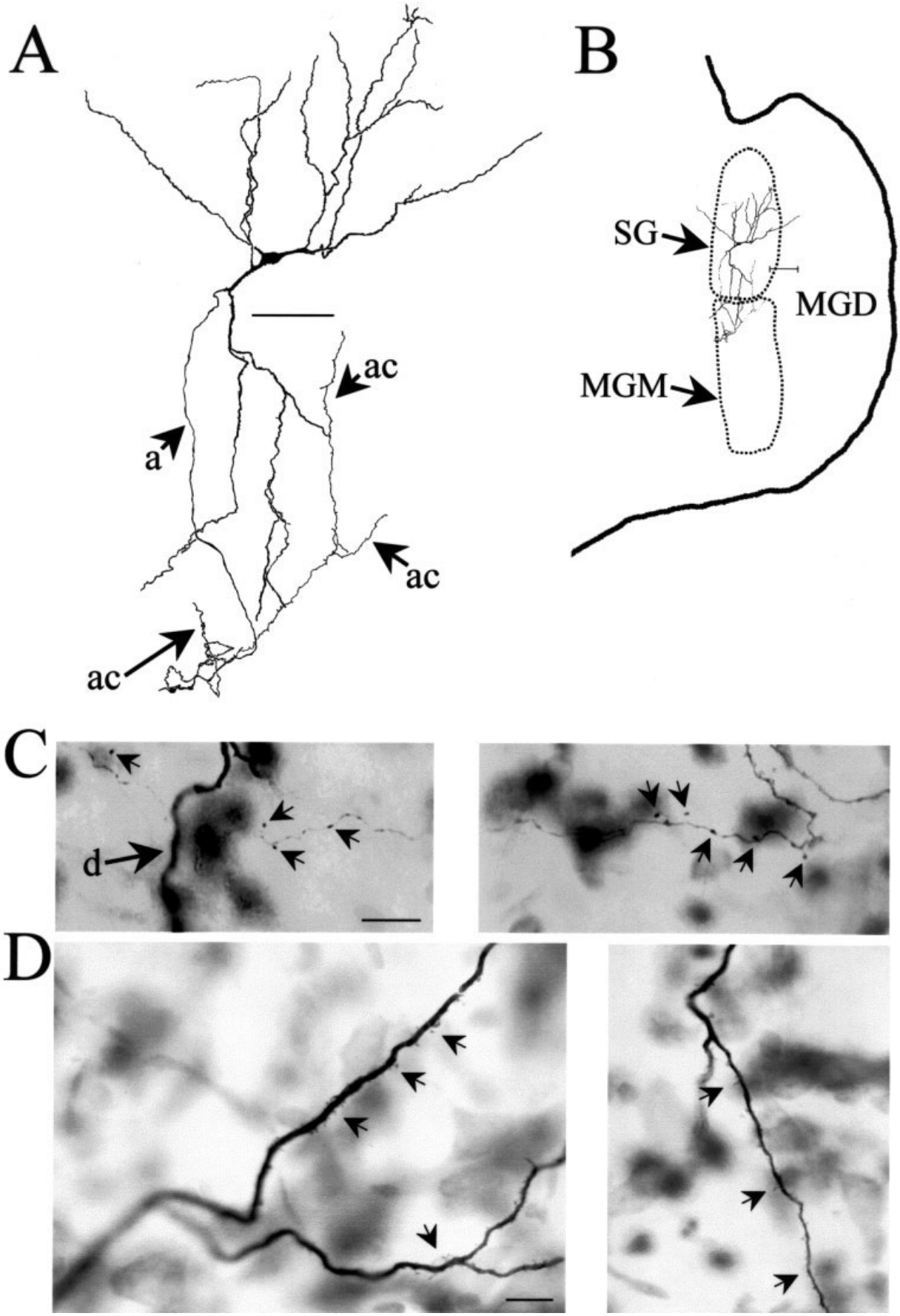

Fig. 4. Elongate cell in a paralaminar nucleus. **A:** Camera lucida drawing of the cell body, dendritic tree, axon (a), and axon collaterals (ac). This cell is also seen in Figure 3 (cell 6). **B:** Location of the cell in the suprageniculate nucleus (SG). **C:** Photomicrographs illustrating several en passant and en terminaux swellings (arrows) along axon collaterals. The micrograph on the left also contains an out-of-focus dendrite (d) of the labeled cell. **D:** Photomicrographs of portions of the dendritic tree illustrating the dendritic spines (arrows). Scale bars = 100 μm in A, 100 μm for B; 10 μm in C (applies to C,D).

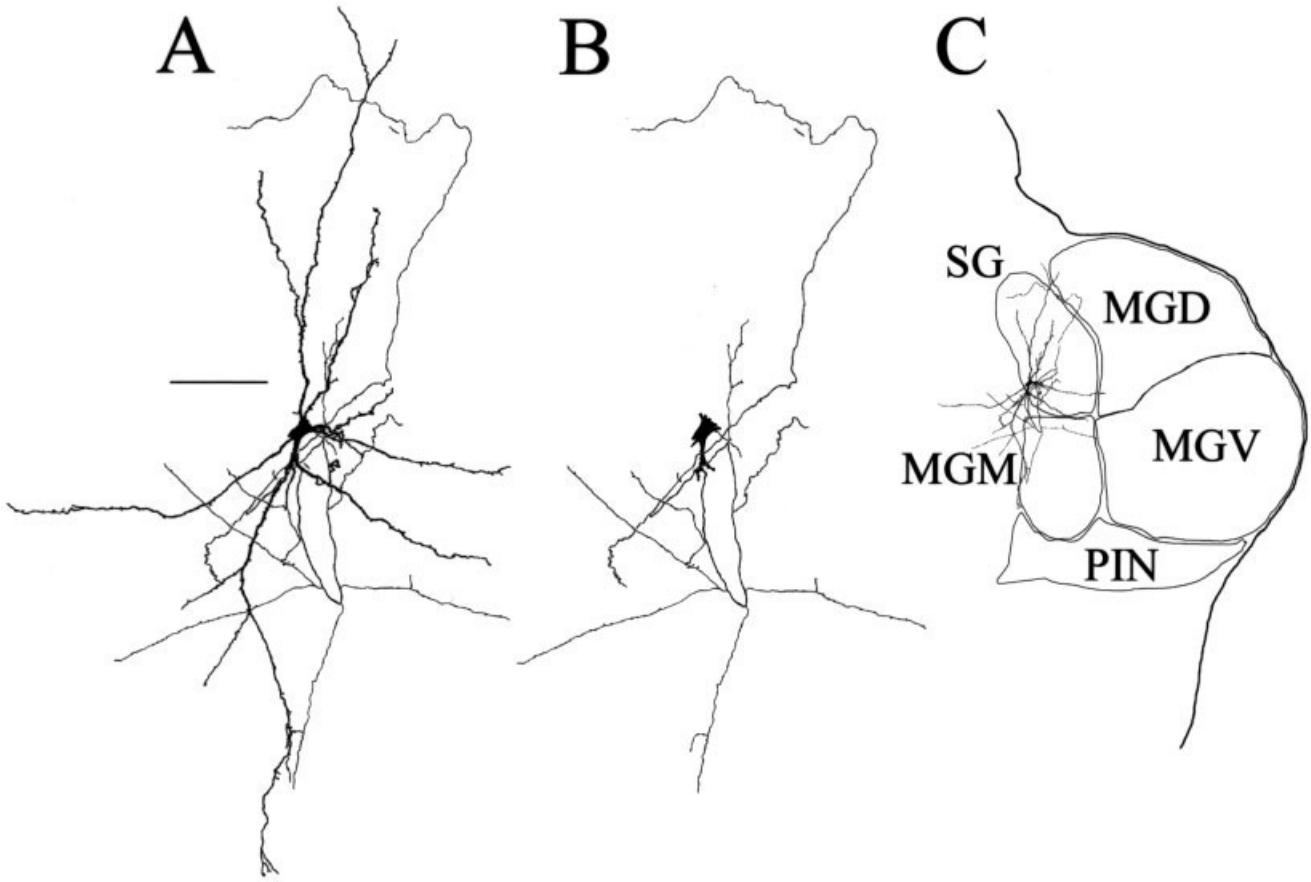

Fig. 5. Elongate cell in a paralaminar nucleus. **A:** Camera lucida drawing of an elongate cell body, dendritic tree, and axon. This cell is also illustrated in Figure 3 (cell 2). **B:** Cell body, main axon, and axon collaterals of the same cell with the dendrites removed. **C:** Location of the cell at the ventromendial border of the suprageniculate nucleus (SG). Scale bar = 100 μm in A (applies to A–B).

significantly larger than those of the MGV/MGD cell population (61.3 ± 10.3 mV, $P < 0.0001$), as were their input resistances (82.6 ± 49.6 mΩ vs. 55.2 ± 31 mΩ, $P < 0.005$).

Bursting response. The most striking response feature of many of the paralaminar cells was the absence or reduction of the low-threshold, voltage-sensitive calcium conductance that elicits the burst firing response that is so prominent in all thalamocortical cells in the MGV and MGD and elsewhere in the sensory thalamus. A typical bimodal spike response of an MGV or MGD cell to depolarizing current pulses at various membrane potentials is illustrated in Figure 6A. At depolarized levels (Fig. 6A, top trace), the cell fires in a sustained, irregular fashion. At more negative levels, the same depolarization activates the calcium burst over a large range of membrane potentials (Fig. 6A, third to fifth traces). Responses shown in Figure 6B,C are examples from two different paralaminar cells. For some paralaminar cells (25%), the cell fired in a regular, sustained fashion at all membrane potentials when the current pulse was suprathreshold (Fig. 6B, top four traces). At more hyperpolarized levels, these cells stopped firing, with no indication of a calcium burst (Fig. 6B, fifth trace), nor could these bursts be elicited at higher current levels at these membrane potentials (not shown). Other paralaminar cells (24%) showed persistent firing at depolarized levels, but with some spike frequency adaptation (Fig. 6C, top four traces). Again, these cells would show little or no indication of a burst at more hyperpolarized levels. Some of these cells with little or no burst response could fire at high sustained rates, sometimes over 400 Hz, when depolarized (Fig. 7A). Paralaminar cells such as those shown in Figure 6B,C also did not display typical rebound burst firing after being hyperpolarized. Figure 7B illustrates the standard response of a cell in MGV or MGD to a hyperpolarizing current pulse as the membrane potential is moved around rest. At a fairly wide range of potentials, the hyperpolarization deactivates the Ca conductance such that when the membrane is repolarized the activated Ca conductance elicits an offset burst. Figure 7C illustrates the response of a paralaminar neuron to a similar set of stimuli. No rebound burst is elicited at any membrane potential.

Other paralaminar cells (44%) did show what appeared to be a calcium burst that generated a series of sodium spikes. Figure 6D,E illustrates two examples. At depolarized levels, these paralaminar cells fired in a regular fashion. As the cells were stepped to more hyperpolarized levels, they could first show an onset response (Fig. 6D, third panel) and then a burst (33%, Fig. 6D, fourth panel) or could show a burst followed by a pause and a resump-

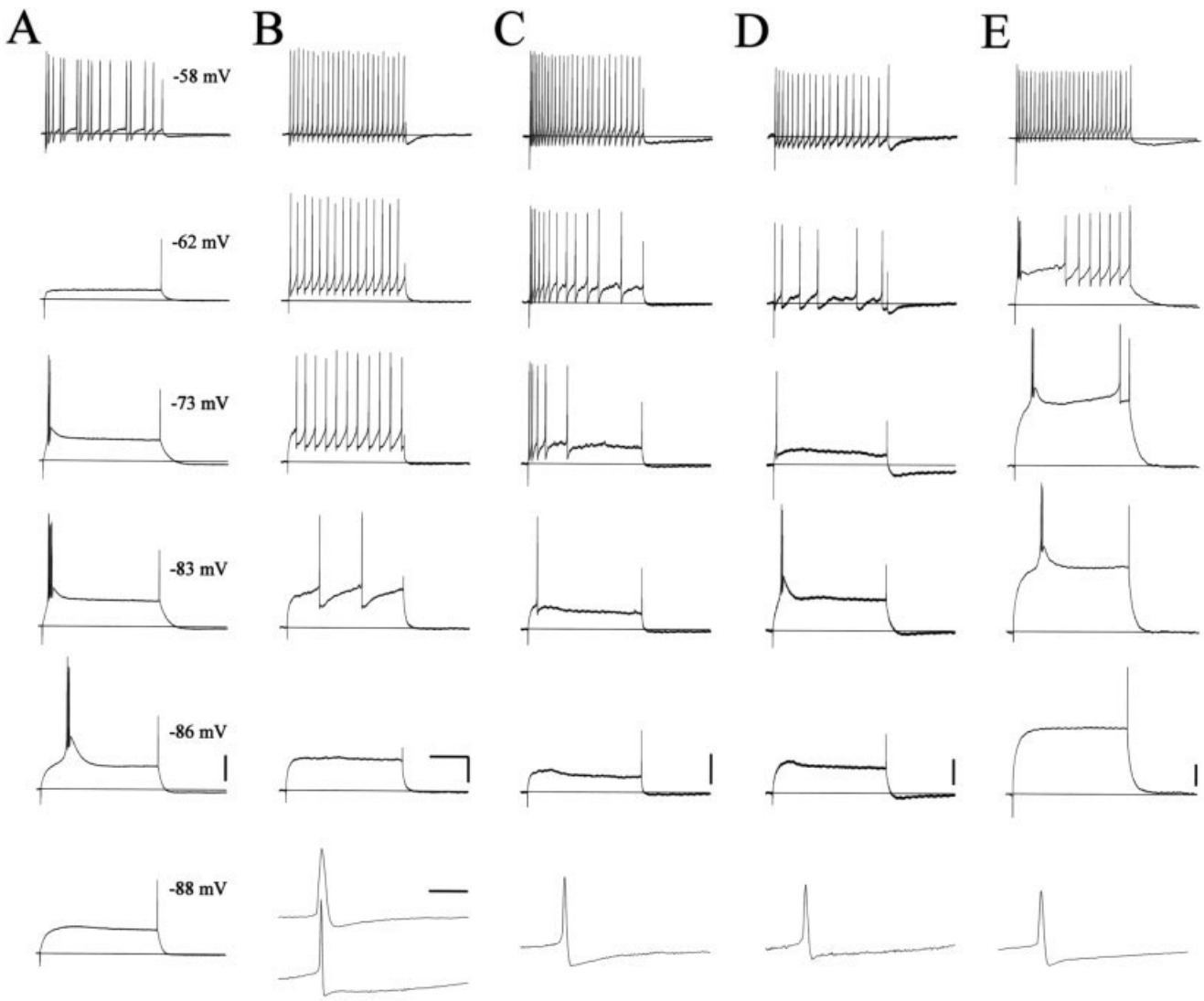

Fig. 6. Comparison of the basic response properties of thalamocortical cells in the MGV and MGD with those of cells in the paralaminar nuclei. **A:** Typical response of a tufted or stellate cell in the MGV or MGD to suprathreshold depolarizing current pulses as the cell was held at different membrane potentials. Voltages next to traces indicate DC level of the cell. **B–D:** Top five traces. Typical responses of paralaminar cells to suprathreshold current pulses as the cells were held at different membrane potentials similar to those indicated in column A. Bottom traces in B compare an action potential from the MGV cell whose response is shown in A (top spike) with an action potential from the paralaminar cell whose response is shown in B (bottom spike). Bottom traces in C, D, and **E** illustrate action potentials from the paralaminar cells in C, D, and E. Time scale bar in row 4 of B = 100 msec and applies to all traces showing response to current pulses. Time scale bar in row 5 of B = 5 msec and applies to all single spike traces at the bottom of B–E. Voltage scale bar in each column = 20 mV and applies to all current injection traces in that column.

tion of sustained activity (11%, Fig. 6E, second panel) and then a burst only (Fig. 6E, fourth panel). Rebound bursts could also be generated in these paralaminar cells (Fig. 7D). We used the area under the rebound bursts as a measure of the burst amplitude and compared these values for paralaminar cells that showed a burst with the TC cells in the MGV/MGD. Paralaminar cells with burst responses had significantly smaller bursts (593.9 ± 390 arbitrary units) than MGV/MGD cells (851.8 ± 301, $P < 0.002$). As might be expected, these smaller paralaminar calcium bursts generated a significantly lower spike rate (206.3 ± 103.2 Hz) than that seen in MGV/MGD cells (264.6 ± 64.2 Hz, $P < 0.002$).

Action potential. Another unique feature of the response of many paralaminar cells was the action potential afterhyperpolarization (AHP); 72% of our MGM cells displayed spikes with biphasic AHPs (bAHPs) consisting of a fast and a slow component, whereas the rest showed monophasic AHPs (mAHPs) like those of MGV/MGD cells. Paralaminar cells with no apparent calcium burst and also those with bursts could display action potentials with either biphasic or monophasic action potentials. Biphasic AHPs are never seen in recordings from MGV/MGD cells (Bartlett and Smith, 1999). The bottom panel in Figure 6B compares the action potential of the MGV TC cell whose responses are seen in Figure 6A (top spike) with one from

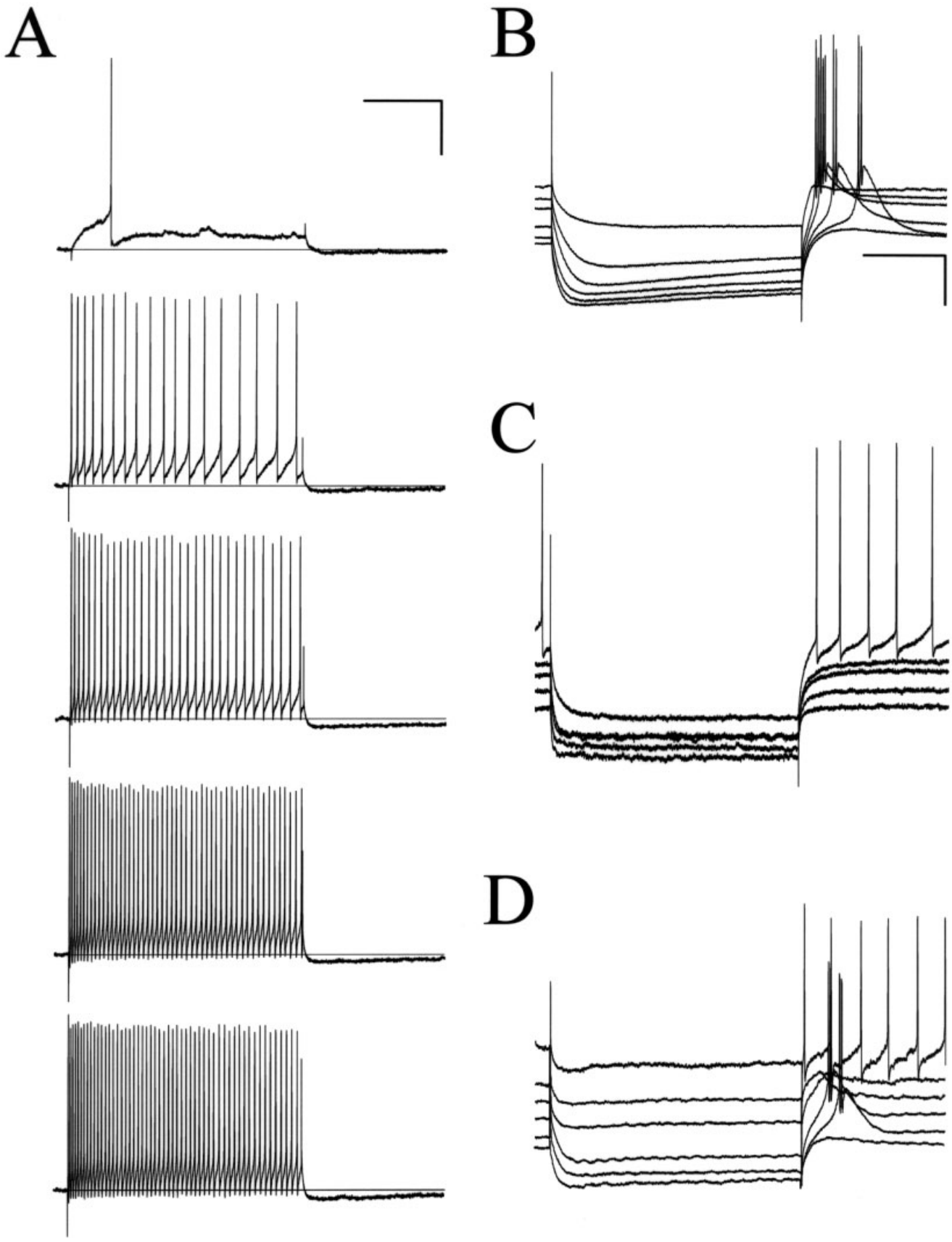

Fig. 7. Sustained firing (A) and rebound responses after hyperpolarizing current pulses (B). **A:** Response of a paralaminar cell to current pulses of increasing current strength (top to bottom). **B:** Typical response of a tufted or stellate cell in the MGV or MGD to hyperpolarizing current pulses as the cell was held at different membrane potentials. The cell shows a rebound burst over a wide range of membrane potentials. **C:** Typical response of some cells in the paralaminar nuclei adjacent to MGB to similar hyperpolarizing current pulses as the cell was held at different membrane potentials. No rebound burst could be elicited at any membrane potential even if the amplitude of the current pulse was increased (not shown) **D:** Response of some cells in an adjacent paralaminar nucleus that did show a calcium burst as the cell was held at different membrane potentials. Scale bars = 20 mV, 100 msec in A; 20 mV, 100 msec in B (applies to B–D).

the paralaminar cell seen in Figure 6B (bottom spike). The bottom panels of Figure 6C–E also illustrate spike waveforms of the other paralaminar cells in these columns. Unlike the MGV cell monophasic spike AHP, three of the four paralaminar cell spikes (B, D, and E) show a slow component of the AHP.

We used the biphasic or monophasic nature of the action potential AHP to divide MGM cells into two groups. We do not know whether this represents a true functional subdivision of cell types, but differences in other features of their physiology led us to make this distinction. First, as described above, a comparison of the rebound burst size for paralaminar cells that showed a calcium conductance (regardless of the nature of their spike AHP) with cells in the MGV/MGD demonstrated that the paralaminar cell calcium conductance was significantly smaller. However, if the paralaminar cells were divided into those with mAHPs or bAHPs, the burst size generated by the cells with mAHPs was comparable to the burst size seen in MGV and MGD cells, whereas the bursts of cells with bAHP was significantly smaller. ANOVA comparisons of the area under the rebound bursts generated by paralaminar cells with mAHPs, by those with bAHPs, and by cells in the MGV/MGD revealed a significant difference [$F(2,93) = 10.9$, $P < 0.0001$]. Post hoc *t*-tests illustrated that the paralaminar cells with mAHPs had rebound bursts whose amplitudes (823 ± 344 arbitrary units) were not significantly different from those of cells in MGV/MGD (859 ± 301), whereas both of these groups had significantly larger bursts than the paralaminar cells with bAHPs (511 ± 374, $P < 0.003$ and $P < 0.0001$). A second feature distinguishing the paralaminar cells with biphasic vs monophasic AHPs was the cells input resistance. As we described above, the paralaminar cell input resistances were significantly different from those of the MGV/MGD cell population, but this was due to the high input resistances of the paralaminar cells with bAHPs. ANOVA evaluation of the means of MGV/MGD, paralaminar bAHP, and paralaminar mAHP cell input resistances showed that there were significant differences [$F(2,120) = 6.56$, $P < 0.002$], but post hoc *t*-tests showed that the paralaminar bAHP cell input resistance (88.4 ± 52.9 mΩ) was significantly different from that of the MGV/MGD cells (55.2 ± 31 mΩ, $P < 0.01$), whereas that of the paralaminar mAHP cell was not. A final feature of the paralaminar cell that led us to make this distinction was action potential duration. ANOVA comparisons followed by post hoc *t*-tests showed no significant differences in the mean values of the MGV/MGD, paralaminar mAHP, or paralaminar bAHP cell action potential half-widths, but those of the paralaminar bAHPs spanned a much larger range (0.16–1.48 msec) than the other groups (0.34–0.9 msec). Spikes with very short (<0.3 msec) half-widths exhibited by several paralaminar cells with bAHPs are comparable to those reported for interneurons in the thalamus (Pape and McCormick, 1995).

In summary, paralaminar cells can show little or no calcium burst and a sustained regular or adaptive firing pattern over a large voltage range. This firing can reach very high rates. Their resting potentials are comparable to those seen in MGV/MGD cells, but their action potentials are larger. Their action potentials can show biphasic or monophasic AHPs. Paralaminar cells that both do and do not show bursting can have either bAHPs or mAHPs. For those that burst, the size of the burst is smaller in those cells with bAHPs. Other unique features of the paralaminar bAHP cells are the higher input resistance, the wide range of action potential durations, and the rate of spiking generated by the burst.

Verification of the calcium conductance. Figures 8 and 9 verify that these bursts in some MGM cells are in fact calcium mediated. Figure 8A shows that reduction of the calcium concentration (lower panel) reduces the amplitude of the bursts (arrows) of a typical TC cell in MGV to depolarizing and hyperpolarizing pulses (n = 7 cells). Likewise, a similar reduction in calcium levels reduces the depolarization- and hyperpolarization-induced bursts (Fig. 8B, arrows) in an MGM cell. For those paralaminar cells with no noticeable burst, the sustained firing would persist when the calcium level was lowered (n = 5 cells) but at an altered rate (Fig. 8C). Nickel has been shown to block/reduce the low-threshold Ca conductance in thalamocortical cells (Hernandez-Cruz and Pape, 1989). Figure 9A illustrates that nickel reduces both the depolarization-induced and the rebound Ca burst in a TC cell in MGD. Figure 9B,D shows representative responses from two cells in the paralaminar nuclei, and in both cases the depolarization-induced and rebound bursts are significantly reduced in the presence of nickel (N = 7). Paralaminar cells with no apparent Ca burst continued to fire in a sustained fashion but with a slightly altered rate (n = 4; Fig. 9C).

Spike AHP. We also wanted to get some idea of the nature of the paralaminar cell spike AHP. At millimolar concentrations, 4AP blocks fast, voltage-sensitive K channels (I_A) used to repolarize action potentials in TC cells in other areas of the thalamus (Huguenard et al., 1991). Bath application of 4AP also affected the repolarization of the paralaminar cell action potentials (n = 5 cells; Fig. 10). This resulted in the abolition of the fast component of the AHP and a widening of the action potential (Fig. 10C). MGM cells also appear to have a potassium conductance not found in the MGV/MGD cell. Apamin blocks the small-conductance Ca^{2+}-activated K^+ channel known as the SK channel (see Castle et al., 1989). This drug had no apparent effect on the spike waveform and response features of the MGB TC cells (Fig. 11A) but decreased the fast and slow components of the paralaminar spike AHP and subsequently increased the firing rate while maintaining some spike frequency adaptation (n = 4 cells; Fig. 11B). In a paralaminar cell with a burst component, the burst response was prolonged by apamin (n = 2; Fig. 11C).

Comparison with intralaminar cells

Intralaminar nuclei are nuclear structures that lie within the internal medullary lamina of the thalamus. Several previously reported features of cells in the parafasicular nucleus (pf), a nucleus in the posterior intralaminar nuclear group, are unique compared with other areas of the thalamus but are similar to those of paralaminar cells (see Discussion). This led us to examine the basic response properties of cells in the intralaminar nuclei to see whether they too showed the unusual physiological characteristics in vitro that we observed in paralaminar cells. We recorded from and labeled a small sample (n = 10) of cells in coronal or horizontal slices containing intralaminar nuclei including pf. Figure 12 illustrates examples of labeled cells in the pf nucleus. As we have shown for many of our labeled paralaminar cells, these cells showed long, sparsely branching dendrites (Fig. 12A,

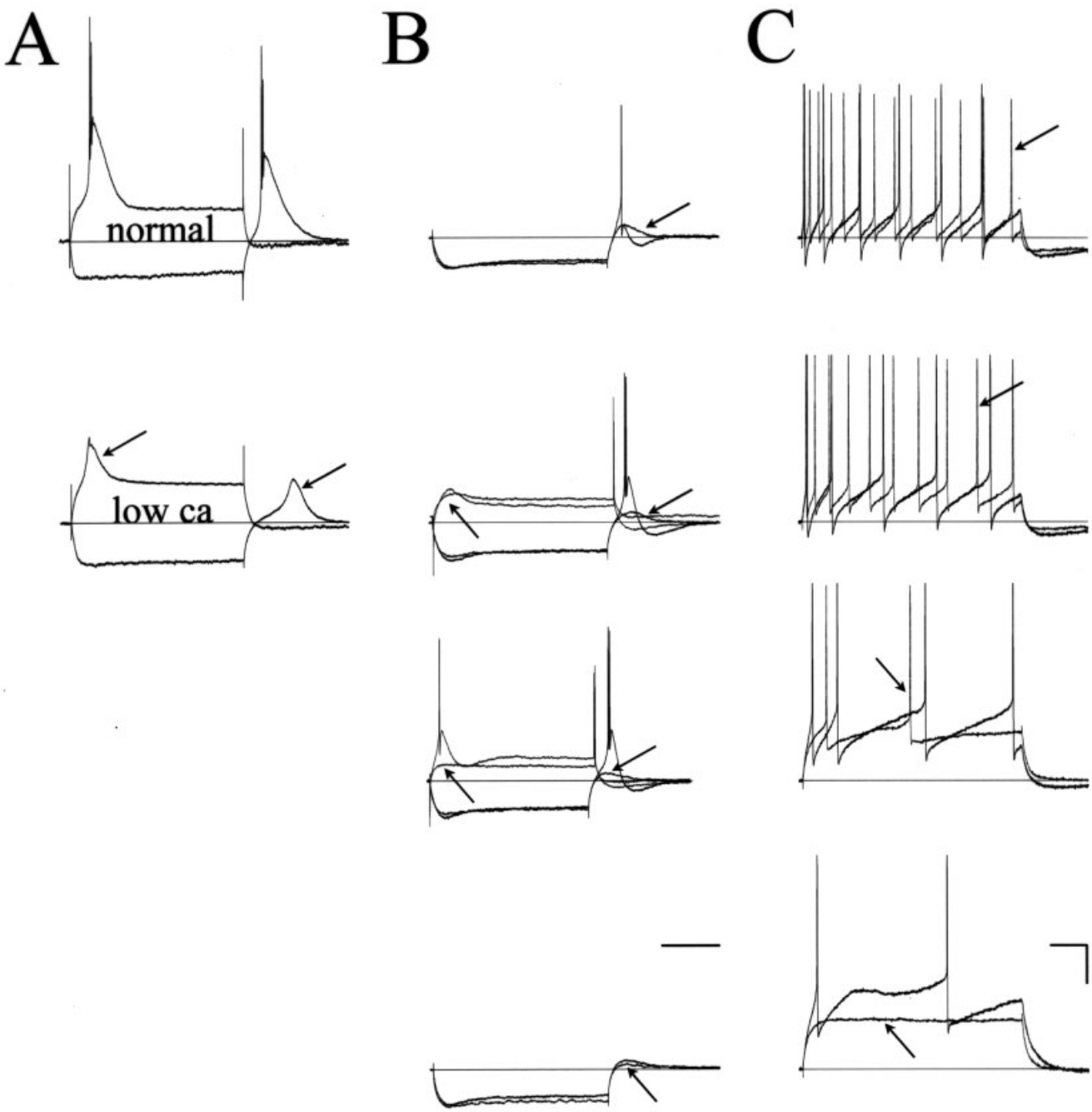

Fig. 8. Comparison of responses in low calcium. **A:** Typical response of a tufted or stellate cell in the MGV or MGD to identical depolarizing and hyperpolarizing current pulses in normal (top) and low calcium (bottom) saline. Arrows highlight reduced Ca bursts in low calcium. **B:** Response of a cell in a paralaminar nucleus to identical hyperpolarizing (top and bottom panels) or both depolarizing and hyperpolarizing pulses (middle two panels) in normal and low-calcium saline as the DC of the cell is moved from depolarized (top panel) to hyperpolarized (bottom panel) levels. Polarizing pulses in normal and low-calcium saline are superimposed on one another. Arrows indicate a reduced calcium burst in the low-Ca saline. **C:** Response of a cell in a paralaminar nucleus without a calcium burst to identical depolarizing current pulses in normal and low-calcium saline as the DC of the cell is moved from depolarized (top panel) to hyperpolarized (bottom panel) levels. Arrows indicate traces/spikes in low-calcium saline. Scale bar = 100 msec in B (applies to A,B). Time scale bar in C = 100 msec. Voltage scale bar in C = 20 mV and applies to all traces.

top left) that may or may not display dendritic spines. Their axons could also give rise to local axon collaterals (Fig. 12A, bottom left). Figure 12B–D illustrates the basic response features of these cells. As described for cells in the paralaminar nuclei, pf cells 1) can have action potentials with biphasic AHPs; 2) can fire in a sustained, reg-

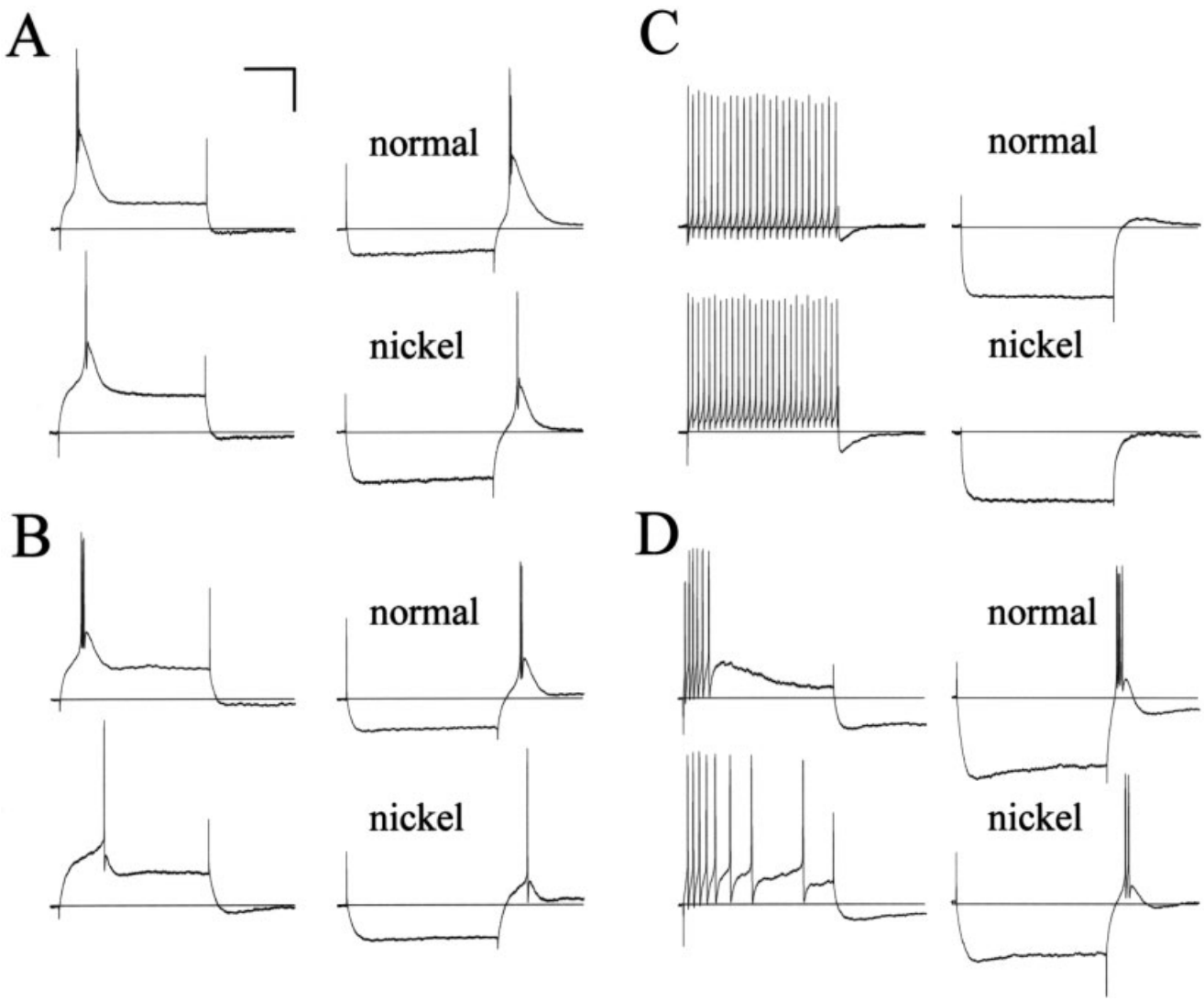

Fig. 9. Comparison of responses in nickel. **A:** Typical response of a tufted or stellate cell in the MGV or MGD to identical depolarizing and hyperpolarizing current pulses in normal saline (top) and saline containing 200 μm nickel (bottom). **B:** Response of a paralaminar cell to identical depolarizing and hyperpolarizing current pulses in normal saline (top) and saline containing nickel (bottom). **C:** Response of another paralaminar cell with no apparent calcium burst to identical depolarizing and hyperpolarizing current pulses in normal saline (top) and saline containing nickel (bottom). **D:** Response of another paralaminar cell with a prolonged Ca burst to identical depolarizing and hyperpolarizing current pulses in normal saline (top) and saline containing nickel (bottom). Scale bars = 100 msec, 20 mV.

ular fashion that can reach high rates with increasing current strength (Fig. 12B) but can also show spike frequency adaptation (not shown); and 3) can have a reduced calcium burst (not shown) or can show very little or no calcium burst to depolarizing (Fig. 12C) or hyperpolarizing (Fig. 12D) current pulses regardless of the membrane potential.

DISCUSSION

Anatomy

Our labeled cell population confirms previous reports that there is diversity in the pool of neurons in the MGM and other paralaminar nuclei adjacent to the MGB. Cells here had multipolar/stellate or elongate dendritic tree configurations and the dendritic branches had or lacked spines. The axons of some cells, usually those with dendritic spines, gave off local axon collaterals, but not all cells with dendritic spines did. Axons of cells labeled in slices can be cut off fairly close to their origin on the cell body or dendritic tree, so it is difficult to know the actual percentage of cells with local collaterals. We also occasionally labeled cells that could be classified as tufted, but the number that could be unequivocally localized to a paralaminar nucleus was low, and they were not included in this report.

An interesting feature of some of our labeled paralaminar cells, perhaps related to their input selection, was their long dendritic branches that could extend into neighboring paralaminar nuclei. Paralaminar nuclei receive in-

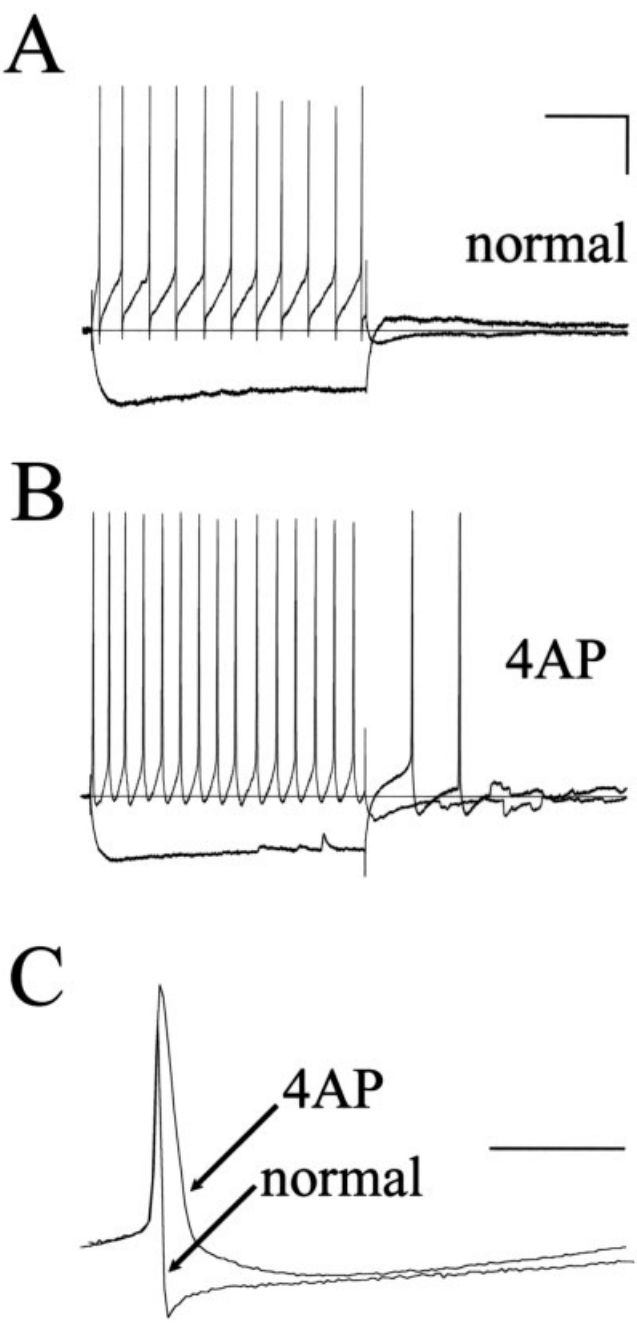

Fig. 10. Responses of a paralaminar cell in 4AP. **A:** Responses to depolarizing and hyperpolarizing pulses of a paralaminar cell that had no significant calcium burst. **B:** Responses of the same cell to identical current pulses while in saline containing 2 mM 4AP. **C:** A spike of the cell in normal saline superimposed on a spike while in saline containing 2 mm 4AP. Scale bars = 20 mV, 100 msec in A (applies to A,B); 5 msec in C.

puts from several auditory and nonauditory areas. These projections do not terminate uniformly over the entire region. For example LeDoux et al. (1987) noted that auditory inputs from the inferior colliculus and somatosensory inputs from spinal cord both innervate the paralaminar nuclei but did not have a large area of overlap. Likewise, Linke (1999) has shown that, although the paralaminar nuclei are all innervated by inputs from both the inferior and the superior colliculi, each paralaminar nucleus has its own unique input pattern. Thus cells with more confined dendrite trees (e.g., stellate/multipolar cells) might be more restricted in what inputs could have an influence, whereas elongate paralaminar cells, such as the ones illustrated in Figures 3–5, would not be subject to such restrictions.

A second unique dendritic feature was the presence of a fairly high concentration of dendritic spines on some of our paralaminar cells but not on others. Spines have been associated with certain forms of synaptic plasticity (Carlisle and Kennedy, 2005), and it is interesting that early reports (Ryugo and Weinberger, 1978; Gerren and Weinberger, 1983) indicated that the MGM is a unique subdivision of MGB in that it is capable of showing plasticity during classical conditioning paradigms. Both studies indicated that synapses of IC inputs onto MGM cells but not onto MGV and MGD cells could show rapid, persistent changes. More recent evidence again has implicated MGM as part of a learning circuit. McEchron et al. (1996) used a classical conditioning paradigm pairing auditory stimuli with a corneal air puff. After training, stimulation of the brachium of the IC but not superior colliculus generated enhanced MGM responses for over 1 hour. Thus, synaptic inputs to the MGM that are activated by the path carrying auditory information to MGM neurons increased in strength as the result of associative conditioning with an acoustic stimulus. Future studies can test the hypothesis that spiny, but not aspiny, paralaminar cells can show lasting changes in synaptic strength.

Another potentially interesting feature of some of the paralaminar cells was the presence of axon collaterals that branched locally in the paralaminar nucleus containing the cell's soma or in a nearby paralaminar nucleus (Figs. 5, 6). These terminals are presumably excitatory. We have preliminary physiological results showing that electrical stimulation of inputs to the paralaminar nuclei from IC, SC, and auditory cortex generate early, direct synaptic events followed by longer latency, indirect excitatory postsynaptic potentials (EPSPs). These later events may be generated by inputs from other activated MGM cells with local collaterals. Similar stimulation of IC and auditory cortex inputs to cells in MGD or MGV elicits direct synaptic events but not longer latency EPSPs, which correlates with the fact that the axons of stellate and tufted cells never give off local collaterals and that the MGM cell collaterals do not appear to stray into MGD or MGV. Thus spike activity of a cell within a paralaminar nucleus can have a direct excitatory effect on neighboring paralaminar cells.

Numerous retrograde labeling studies (see, e.g., Ottersen and Ben-Ari, 1979; LeDoux et al., 1985, 1987, 1990; Winer and Larue, 1987; Scheel, 1988; Roger and Arnault, 1989; Clerici and Coleman, 1990; Moriizumi amd Hattori, 1992; Brett et al., 1994; Shammah-Lagnado et al., 1996; Doron and LeDoux, 1999; Linke, 1999; Linke et al., 1999; Winer et al., 1999, 2002; Kimura et al., 2003) have shown that cells in the paralaminar nuclei project to several sites, including the cerebral cortex, amygdala, basal ganglia, and IC. Unfortunately, because of the incomplete filling of cellular processes, none of these reports described features of the dendritic trees or local axonal branching pattern of the backfilled paralaminar cells, so we do not

know whether any of the cell types reported here (stellate/elongate, spines/no spines, axon collaterals/no collaterals) project to a unique target.

Physiology

We have shown that cells in the MGM and adjacent paralaminar nuclei have unusual basic response features compared with reports of cells elsewhere in the thalamus. The most striking feature was the reduction or apparent lack of a low-threshold voltage-sensitive Ca conductance in many cells. The vast majority of reports describing recordings from thalamic cells include this conductance as a regular feature of all thalamocortical neurons, and a great deal of significance has been assigned to its influence on the output of the cell. The only region of the thalamus where an apparent lack of this Ca conductance has been reported is the γ-aminobutyric acid (GABA)-ergic thalamic reticular nucleus (TRN). In vivo intracellular recordings from cells here (Contreras et al., 1992) were classified as type I or II based on the ability (type I) or lack thereof (type II) to generate a high-frequency burst of spikes. Subsequent in vitro recordings (Brunton and Charpak, 1997) showed a lack or reduction of the low-threshold Ca conductance in the type II TRN neurons and, as with our paralaminar cells, sustained regular firing to suprathreshold currents at all membrane potentials. The only other report of cells in the thalamus whose basic intrinsic physiology differs somewhat from the norm is a report from Li et al. (2003) on cells in the rat lateral posterior nucleus (LPN), a "higher order" visual thalamic nucleus. Unlike our paralaminar cells, LPN cells showed the typical thalamocortical cell morphology, and all displayed the low-threshold calcium conductance. However, unlike the standard TC cell in "first-order thalamic nuclei," some cells had a "regular spiking" mode and short-duration action potentials with biphasic AHPs similar to those seen in many of our paralaminar cells. The authors also noted some cells that displayed a "clustered spiking," defined as a firing mode in which depolarizing current elicited epochs of high-frequency bursts of firing not caused by the low-threshold Ca conductance. We have also seen cases of this "clustered spiking" response type in the paralaminar nuclei but do not yet have a large enough sample of labeled, positively identified cells to report any details with confidence.

Paralaminar vs. intralaminar cells

Intralaminar nuclei are nuclear structures that lie within the internal medullary lamina of the thalamus. It has been suggested that cells in one of the posterior intralaminar nuclei, the pf, supply the striatum with information about behaviorally significant sensory events, which it uses to help modulate the animal's motor response (see, e.g., Van der Werf et al., 2002; Smith et al., 2004). We recorded from and labeled a small population of

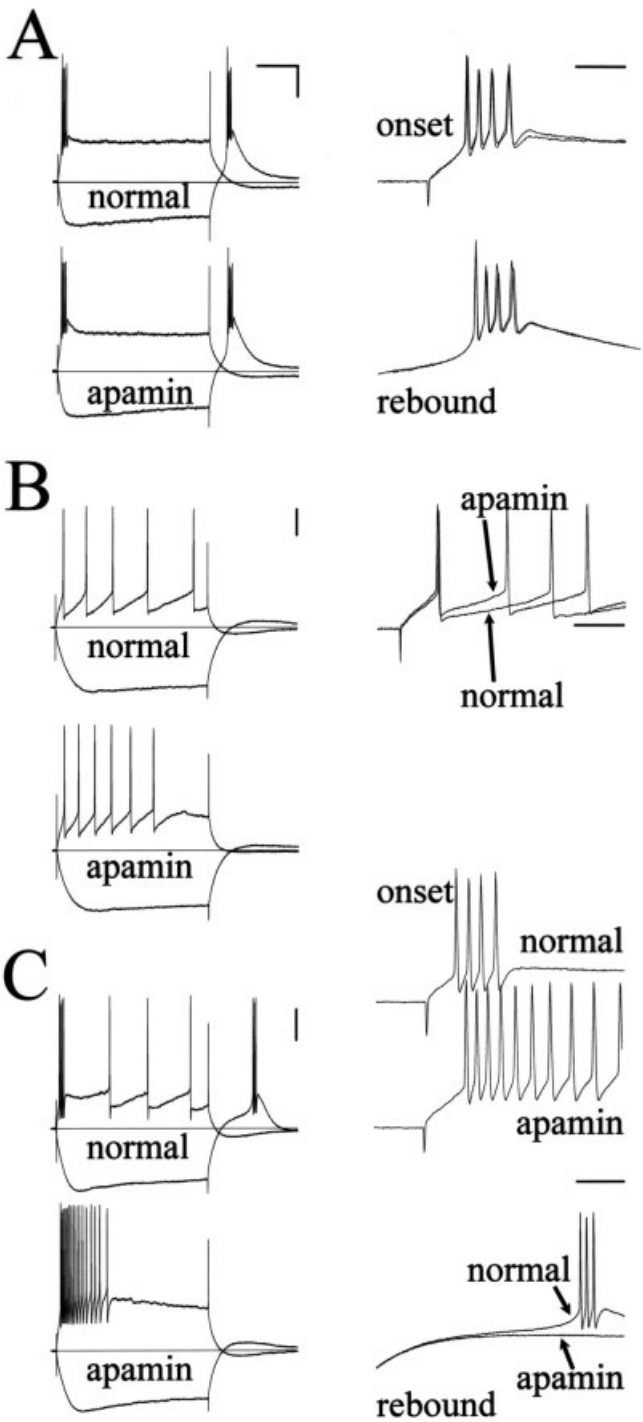

Fig. 11. Comparison of responses in apamin. **A:** Left side: Typical response of a tufted or stellate cell in the MGV or MGD to identical depolarizing and hyperpolarizing current pulses in normal (top) and saline containing 20 nM apamin (bottom). Right side: Superimposed onset (top) and rebound (bottom) bursts in normal and saline containing apamin showing no change. **B:** Left side: Response of a paralaminar cell that had no calcium burst to identical depolarizing and hyperpolarizing current pulses in normal (top) and saline containing apamin (bottom). Right side: Superimposed responses at the onset of the depolarization in normal and saline containing apamin. **C:** Left side: Response of a paralaminar cell that had a calcium burst to identical depolarizing and hyperpolarizing current pulses in normal (top) and saline containing apamin (bottom). Right side: Onset (top, traces offset from one another) and rebound (bottom, responses superimposed) responses in normal and saline containing apamin. Voltage scale bar = 20 mV. Time scale bar in A = 100 msec and applies to left column in A, B and C. Scale bar in right column in A = 10 msec (applies to all traces in right column).

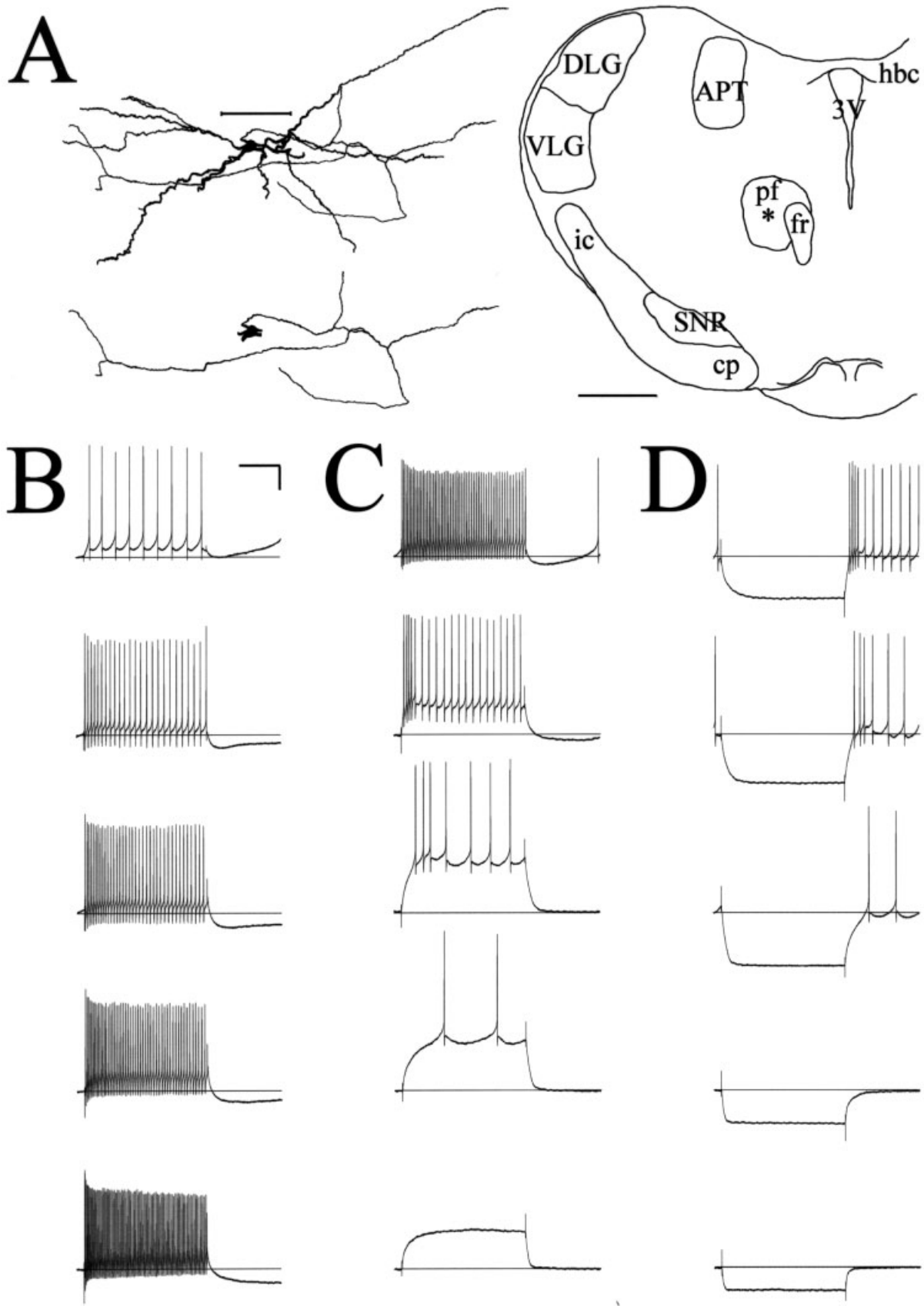

Fig. 12. Cell in the parafascicular nucleus. **A:** Top left: Camera lucida drawing of the cell body, dendritic tree, and axon. Bottom left: Drawing of the cell body, main axon, and axon collaterals of the same cell with the dendrites removed. Right: Location of the cell (asterisk) in the parafascicular nucleus. **B:** Response of the cell shown in A to current pulses of increasing current strength (top to bottom). **C:** Response of the same cell to suprathreshold depolarizing current pulses as the cell was held at different membrane potentials. **D:** Response of the same cell to hyperpolarizing current pulses as the cell was held at different membrane potentials. APT, anterior pretectal nucleus; cp, cerebral peduncle; DLG, dorsal lateral geniculate nucleus; fr, fasciculus retroflexus; hbc, habenular commissure; ic, internal capsule; PF, parafascicular thalamic nucleus; SNR, substantia nigra pars reticulata; VLG, ventral lateral geniculate nucleus; 3V, third ventricle. Scale bars = 100 μm in A at left; 1 mm at right; 20 mV, 100 msec in B (applies to B–D).

pf cells. This was motivated by previous reports describing features of cells in the rat pf and paralaminar nuclei that were similar. First, cells in both pf and paralaminar nuclei can project to the striatum (Herkeham, 1980; LeDoux et al., 1985; Feger et al., 1994; Deschenes et al., 1996; Vercelli et al., 2003; Castle et al., 2005). LeDoux et al. (1985) noted that retrogradely labeled cells from the caudate-putamen formed a continuous stream of cells running from paralaminar nuclei rostromedially into the posterior intralaminar nuclei. Second, in vivo recordings from pf and paralaminar nuclei showed that cells can be multimodal, responding to auditory and somatosensory stimuli with responses that rapidly adapt to repeated auditory stimuli (Bordi and LeDoux, 1994a,b; Matsumoto et al., 2001). Third, work by Scheibel and Scheibel (1967) and Deschenes et al. (1996) described "nonspecific" neurons in the intralaminar nuclei that were "reticular-like" with long, scarcely ramifying spine bearing dendrites and axons that gave off locally ramifying axon collaterals. Deschênes et al. (1996) speculated that these reticular-like intralaminar cells with an anatomy that differed so drastically from the stereotypical TC cell in relay nuclei could also differ in their physiology. All of these observations motivated us to record from pf cells in vitro, and we noted similarities in our pf and paralaminar cells. As with paralaminar cells, pf cells could lack or have a reduced low-threshold calcium conductance and could show regular, sustained firing and action potentials with biphasic AHPs. In agreement with previous descriptions, these cells also resembled the elongate paralaminar cells with their long, sparsely branching dendrites, which may or may not be spiny, and their axons, which may display local collateral branches. We propose, based on these similarities, that at least some of our elongate paralaminar cells could be thalamostriatal or at least integrate and transmit synaptic inputs in a similar fashion.

Burst function

To begin to try to interpret why bursts are reduced or absent in paralaminar cells, it might be helpful first to understand their function in areas of the thalamus where they are ubiquitous. In the visual thalamus, thalamocortical neuron bursts have been postulated to be involved in the generation of synchronized sleep rhythms (Livingstone and Hubel, 1981; Steriade et al., 1993). More recent findings that cells in the visual thalamus of the alert, awake cat also respond in a burst fashion (Guido and Weyand, 1995; Reinagel et al., 1999; Weyland et al., 2001; Lesica and Stanley, 2004) have dampened enthusiasm for this idea. The current thinking is that cells in burst mode are better able to detect near-threshold visual stimuli (see Sherman, 2001). Another observation that may be relevant to thalamic burst function in the visual system was made by Swadlow and Gusev (2003), who noted that a spike burst was more efficient at eliciting a spike in a cortical neuron receiving this input.

There is less information regarding the function of the bursting response in the auditory thalamus in vivo. Yu et al. (2004) recorded intracellularly from cells in the guinea pig MGB. By using current injection, they changed the membrane potential of cells and showed that the driven response to an auditory stimulus could change from burst to tonic firing modes. The burst firing response occurred at hyperpolarized levels and was almost certainly due to the low-threshold calcium conductance. Unfortunately, they did not report the MGN location of the cells that illustrated this membrane potential-dependent response change. Other extracellular recording studies (He and Hu, 2002; Massaux et al., 2004) found that the proportion of burst firing varied depending on the animal's state and the electrode location and that bursts were detected in awake, anesthetized or sleeping animals, during spontaneous or sound-driven responses and in all areas of the MGB (including MGM). Massaux et al. (2004) noted that, in awake guinea pigs, the burst component of responses to tones occurred preferentially at or around the cell's best frequency and that response latency and variability of the response latency were both reduced for the bursts. This would indicate that the burst response might give a more selective and accurate representation of sound frequency to postsynaptic targets. All of this would provide very indirect evidence that paralaminar cells lacking bursts might be less likely to respond synchronously as a group or respond to near-threshold stimuli and less likely to have narrow, more refined response areas or to activate their postsynaptic target with a high degree of reliability.

Another way of attempting to determine why bursts are reduced or absent in MGM cells would be to try to relate how such cells might be better able to perform their proposed function. One set of paralaminar cells, those that project to the amygdala, is part of the pathway responsible for the behavioral and autonomic events elicited by the conditioned fear response (LeDoux et al., 1988; LeDoux, 1995; LeDoux and Muller, 1997). LeDoux and colleagues noted that, within this pathway, long-term potentiation (LTP)-like associative processes occur during fear conditioning and may underlie the long-term associative plasticity that constitutes memory of the conditioning experience. Lesion, tracer, and recording experiments have shown that paralaminar nuclei are the interface between the anterolateral amygdala (AL) and the ascending auditory system (LeDoux et al., 1986, 1990a,b; Clugnet et al., 1990). Further experiments documented that amygdalar responses to auditory inputs are enhanced by electrical stimulation specifically applied to the medial MGB or by prior conditioning of the auditory stimulus (Clugnet and LeDoux, 1990; Rogan and LeDoux, 1995; Quirk et al., 1995). It should be noted that the electrical stimuli used by Clugnet and LeDoux to induce LTP were trains of 30 pulses at 400 Hz. Cells in a calcium burst mode could not follow such a rapid stimulus given the long refractory period (around 200 msec) of the underlying conductance (Jahnsen and Llinas, 1984a). Cells with no burst and an ability to respond steadily at high rates (see Fig. 7A) could follow such a stimulus.

Another function of the paralaminar nuclei is to activate 40-Hz oscillations in the auditory cortex. Human studies (Llinas and Ribary, 1993; Joliot et al., 1994) showed that 40-Hz oscillations could reflect cognitive processing of auditory stimuli and the "temporal binding" of sensory stimuli into a single experience. *Temporal binding* refers to the conscious binding together of sensory events that occur during a particular time as a single experience, and the 40-Hz oscillation is "required" for this to occur. Barth and McDonald (1996) reported that gamma oscillations occurred spontaneously or could be evoked in auditory cortex by auditory stimuli. They further showed that auditory thalamus could modulate these oscillations. Electrically stimulating of MGV or MGD inhibited the 40-Hz cortical response, whereas stimulation of the me-

dial aspect of the auditory thalamus elicited it. The finding suggests a functional role for MGM in cognition. Again, in these experiments, the electrical stimulation used to evoke the cortical 40-Hz oscillations was at a high rate (500 msec duration at 500 Hz), which could not be followed by cells in bursting mode but might be by cells capable of high sustained firing.

Apamin-sensitive conductance

We have shown that some paralaminar cells possess the apamin-sensitive SK-type calcium-activated K channel, whereas TC cells in the MGV and MGD do not. We also showed that the SK channel is controlling some aspects of the firing properties of the paralaminar cells. Blocking the channel had little or no effect on the MGV/MGD spike response (see Fig. 11A) but prolonged the spike response of paralaminar cells that did possess a Ca burst (Fig. 11B) and increased firing frequency of a paralaminar cell that did not show a calcium burst (Fig. 11C). One of the SK channel proteins is highly expressed in the thalamic reticular nucleus (Sailer et al., 2002), where channel blockade by apamin affected neuronal excitability (Bal and McCormick, 1993, Debarbieux et al., 1998), so both TRN and paralaminar cells seem to possess this channel. Another observation on the TRN SK channel is that it was affected by the intravenous anesthetic propofol (Ying and Goldstein, 2005). Propofol also blocks auditory evoked focal gamma band oscillations (40-Hz oscillatory electrical activity) in auditory cortex, and stimulation of either the TRN (Macdonald et al., 1998) or the medial division of the MGB (Barth and MacDonald, 1996) elicits this 40-Hz cortical oscillation. Perhaps the auditory TRN, its connection to the MGM, and the MGM projection to cortex are important components of the 40-Hz activation circuitry and the propofol effect on the SK channel at one or both locations explains its effect on the oscillation. Recently, the SK channel has also been implicated in LTP. Faber et al. (2005) showed that activation of glutamatergic synapses in the amygdala caused calcium influx through N-methyl-D-aspartate channels that activated SK channels and shunted the EPSP. Apamin blockade of this channel allowed synaptic events to summate and generate an enhanced LTP. It is interesting to note that at least some MGM cells express the SK channel and that this is the only part of the MGB where potentiation of synaptic events has been found (Ryugo and Weinberger, 1978; Gerren and Weinberger, 1983; McEchron et al., 1996). Thus, just as low-voltage Ca channels can act as "sensory gates" in first-order TC neurons, the SK channels in some paralaminar cells may act as a "learning gate."

In conclusion, some cells in MGM and surrounding paralaminar nuclei have been shown to possess unique features distinguishing them from the majority of other cells in the dorsal thalamus but linking them with cells in intralaminar thalamic nuclei (and the thalamic reticular nucleus). It will be of great interest to determine which of the various cells in the paralaminar nuclei surrounding the medial geniculate nuclei project to their target structures and how these unique anatomical and physiological features that we have described here aid them in the completion of their tasks.

LITERATURE CITED

Aghajanian GK, Rasmussen K. 1989. Intracellular studies in the facial nucleus illustrating a simple new method for obtaining viable motoneurons in adult rat brain slices. Synapse 3:331–338.

Arnault P, Roger M. 1987. The connections of the peripeduncular area studied by retrograde and anterograde transport in the rat. J Comp Neurol 258:463–476.

Arnault P, Roger M. 1990. Ventral temporal cortex in the rat: connections of secondary auditory areas Te2 and Te3. J Comp Neurol 302:110–123.

Bal T, McCormick DA. 1993. Mechanisms of oscillatory activity in guinea-pig nucleus reticularis thalami in vitro: a mammalian pacemaker. J Physiol 468:669–691.

Barth DS, MacDonald KD. 1996. Thalamic modulation of high-frequency oscillating potentials in auditory cortex. Nature 383:78–81.

Bartlett EL, Smith PH. 1999. Anatomical, intrinsic, and synaptic properties of dorsal and ventral division neurons in the rat medial geniculate body. J Neurophysiol 81:1999–2006.

Bartlett EL, Smith PH. 2002. Effects of paired-pulse and repetitive stimulation of inferior colliculus axons on thalamocortical neurons in the rat medial geniculate body. Neuroscience 113:957–974.

Benedek G, Pereny J, Kovacs G, Fischer-Szatmari L, Katoh YY. 1997. Visual, somatosensory, auditory and nociceptive modality properties in the feline suprageniculate nucleus. Neuroscience 78:179–189.

Bordi F, LeDoux JE. 1994a. Response properties of single units in areas of rat auditory thalamus that project to the amygdala. I. Acoustic discharge patterns and frequency receptive fields. Exp Brain Res 98:261–274.

Bordi F, LeDoux JE. 1994b. Response properties of single units in areas of rat auditory thalamus that project to the amygdala. II. Cells receiving convergent auditory and somatosensory inputs and cells antidromically activated by amygdala stimulation. Exp Brain Res 98:275–286.

Brett B, Di S, Watkins L, Barth DS. 1994. A horseradish peroxidase study of parallel thalamocortical projections responsible for the generation of mid-latency auditory-evoked potentials. Brain Res 647:65–75.

Brunton J, Charpak S. 1997. Heterogeneity of cell firing properties and opioid sensitivity in the thalamic reticular nucleus. Neuroscience 78: 303–307.

Carlisle HJ. Kennedy MB. 2005. Spine architecture and synaptic plasticity. Trends Neurosci 28:182–187.

Castle NA, Haylett DG, Jenkinson DH. 1989. Toxins in the characterization of potassium channels. Trends Neurosci 12:59–65.

Castle M, Aymerich MS, Sanchez-Escobar C, Gonzalo N, Obeso JA, Lanciego JL. 2005. Thalamic innervation of the direct and indirect basal ganglia pathways in the rat: ipsi- and contralateral projections. J Comp Neurol 483:143–153.

Clerici WJ, Coleman JR. 1990. Anatomy of the rat medial geniculate body: I. Cytoarchitecture, myeloarchitecture, and neocortical connectivity. J Comp Neurol 297:14–31.

Clerici WJ, McDonald AJ, Thompson R, Coleman JR. 1990. Anatomy of the rat medial geniculate body: II. Dendritic morphology. J Comp Neurol 297:32–54.

Clugnet MC, LeDoux JE, Morrison SF. 1990. Unit responses evoked in the amygdala and striatum by electrical stimulation of the medial geniculate body. J Neurosci 10:1055–1061.

Contreras D, Curro Dossi R, Steriade M. 1992. Bursting and tonic discharges in two classes of reticular thalamic neurons. J Neurophysiol 68:973–977.

Debarbieux F, Brunton J, Charpak S. 1998. Effect of bicuculline on thalamic activity: a direct blockade of IAHP in reticularis neurons. J Neurophysiol 79:2911–2918.

Deschênes M, Bourassa J, Doan VD, Parent A. 1996. A single-cell study of the axonal projections arising from the posterior intralaminar thalamic nuclei in the rat. Eur J Neurosci 8:329–343.

Doron NN, LeDoux JE. 1999. Organization of projections to the lateral amygdala from auditory and visual areas of the thalamus in the rat. J Comp Neurol 412:383–409.

Doron NN, LeDoux JE. 2000. Cells in the posterior thalamus project to both amygdala and temporal cortex: a quantitative retrograde double-labeling study in the rat. J Comp Neurol 425:257–274.

Feger J, Bevan M, Crossman AR. 1994. The projections from the parafascicular thalamic nucleus to the subthalamic nucleus and the striatum arise from separate neuronal populations: a comparison with the corticostriatal and corticosubthalamic efferents in a retrograde fluorescent double-labelling study. Neuroscience 60:125–132.

Gerren RA, Weinberger NM. 1983. Long term potentiation in the magnocellular medial geniculate nucleus of the anesthetized cat. Brain Res 265:138–142.

Guido W, Weyand T. 1995. Burst responses in thalamic relay cells of the awake behaving cat. J Neurophysiol 74:1782–1786.

He J, Hu B. 2002. Differential distribution of burst and single-spike responses in auditory thalamus. J Neurophysiol 88:2152–2156.

Herkenham M. 1980. Laminar organization of thalamic projections to the rat neocortex. Science 207:532–535.

Hernandez-Cruz A, Pape HC. 1989. Identification of two calcium currents in acutely dissociated neurons from the rat lateral geniculate nucleus. J Neurophysiol 61:1270–1283.

Hicks TP, Stark CA, Fletcher WA. 1986. Origins of afferents to visual suprageniculate nucleus of the cat. J Comp Neurol 246:544–554.

Hu B. 1995. Cellular basis of temporal synaptic signaling: an in vitro electrophysiological study in rat auditory thalamus. J Physiol 483:167–182.

Huguenard JR, Coulter DA, Prince DA. 1991. A fast transient potassium current in thalamic relay neurons: kinetics of activation and inactivation. J Neurophysiol 66:1304–1315.

Jahnsen H, Llinas R. 1984a. Voltage-dependent burst-to-tonic switching of thalamic cell activity: an in vitro study. Arch Ital Biol 122:73–82.

Jahnsen H, Llinas R. 1984b. Electrophysiological properties of guinea-pig thalamic neurones: an in vitro study. J Physiol 349:205–226.

Joliet M, Ribary U, Llinas R. 1994. Human oscillatory brain activity near 40 Hz coexists with cognitive temporal binding. Proc Natl Acad Sci U S A 91:11748–11751.

Jones EG. 1998a. A new view of specific and nonspecific thalamocortical connections. Adv Neurol 77:49–71.

Jones EG. 1998b. Viewpoint: the core and matrix of thalamic organization. Neuroscience 85:331–345.

Kharazia VN, Weinberg RJ. 1994. Glutamate in thalamic fibers terminating in layer IV of primary sensory cortex. J Neurosci 14:6021–6032.

Kimura A, Donishi T, Sakoda T, Hazama M, Tamai Y. 2003. Auditory thalamic nuclei projections to the temporal cortex in the rat. Neuroscience 117:1003–1016.

LeDoux JE. 1995. Emotion: clues from the brain. Annu Rev Psychol 46: 209–235.

LeDoux JE, Muller J. 1997. Emotional memory and psychopathology. Philos Trans R Soc Lond B Biol Sci 352:1719–1726.

LeDoux JE, Iwata J, Cicchetti P, Reis DJ. 1988. Different projections of the central amygdaloid nucleus mediate autonomic and behavioral correlates of conditioned fear. J Neurosci 8:2517–2529.

LeDoux JE, Sakaguchi A, Reis DJ. 1984. Subcortical efferent projections of the medial geniculate nucleus mediate emotional responses conditioned to acoustic stimuli. J Neurosci 4:683–698.

LeDoux JE, Ruggiero DA, Reis DJ. 1985. Projections to the subcortical forebrain from anatomically defined regions of the medial geniculate body in the rat. J Comp Neurol 242:182–213.

LeDoux JE, Iwata J, Cicchetti P, Reis DJ. 1986. Different projections of the central amygdaloid nucleus mediate autonomic and behavioral correlates of conditioned fear. J Neurosci 8:2517–2529.

LeDoux JE, Ruggiero DA, Forest R, Stornetta R, Reis DJ. 1987. Topographic organization of convergent projections to the thalamus from the inferior colliculus and spinal cord in the rat. J Comp Neurol 264: 123–146.

Lesica NA, Stanley GB. 2004. Encoding of natural scene movies by tonic and burst spikes in the lateral geniculate nucleus. J Neurosci 24: 10731–10740.

Li J, Bickford ME, Guido W. 2003. Distinct firing properties of higher order thalamic relay neurons. J Neurophysiol 90:291–299.

Linke R. 1999. Organization of projections to temporal cortex originating in the thalamic posterior intralaminar nucleus of the rat. Exp Brain Res 127:314–320.

Linke R, Schwegler H. 2000. Convergent and complementary projections of the caudal paralaminar thalamic nuclei to rat temporal and insular cortex. Cereb Cortex 10:753–771.

Linke R, De Lima AD, Schwegler H, Pape HC. 1999. Direct synaptic connections of axons from superior colliculus with identified thalamoamygdaloid projection neurons in the rat: possible substrates of a subcortical visual pathway to the amygdala. J Comp Neurol 403:158–170.

Linke R, Braune G, Schwegler H. 2000. Differential projection of the posterior paralaminar thalamic nuclei to the amygdaloid complex in the rat. Exp Brain Res 134:520–532.

Linke R, Faber-Zuschratter H, Seidenbecher T, Pape HC. 2004. Axonal connections from posterior paralaminar thalamic neurons to basomedial amygdaloid projection neurons to the lateral entorhinal cortex in rats. Brain Res Bull 63:461–469.

Livingstone MS, Hubel DH. 1993. Effects of sleep and arousal on the processing of visual information in the cat. Nature 291:554–561.

Llinas R, Ribary U. 1993. Coherent 40-Hz oscillation characterizes dream state in humans. Proc Natl Acad Sci U S A 90:2078–2081.

Macdonald KD, Fifkova E, Jones MS, Barth DS. 1998. Focal stimulation of the thalamic reticular nucleus induces focal gamma waves in cortex. J Neurophysiol 79:474–477.

Massaux A, Dutrieux G, Cotillon-Williams N, Manunta Y, Edeline JM. 2004. Auditory thalamus bursts in anesthetized and non-anesthetized states: contribution to functional properties. J Neurophysiol 91:2117–2134.

Matsumoto N, Minamimoto T, Graybiel AM, Kimura M. 2001. Neurons in the thalamic CM-Pf complex supply striatal neurons with information about behaviorally significant sensory events. J Neurophysiol 85:960–976.

McEchron MD, Green EJ, Winters RW, Nolen TG, Schneiderman N, McCabe PM. 1996. Changes of synaptic efficacy in the medial geniculate nucleus as a result of auditory classical conditioning. J Neurosci 16: 1273–1283.

McMullen NT, de Venecia RK. 1993. Thalamocortical patches in auditory neocortex. Brain Res 620:317–322.

Mitani A, Itoh K, Nomura S, Kudo M, Kaneko T, Mizuno N. 1984. Thalamocortical projections to layer I of the primary auditory cortex in the cat: a horseradish peroxidase study. Brain Res 310:347–350.

Mitani A, Itoh K, Mizuno N. 1987. Distribution and size of thalamic neurons projecting to layer I of the auditory cortical fields of the cat compared with those projecting to layer IV. J Comp Neurol 257:105–121.

Morest DK. 1964. The neuronal architecture of the medial geniculate body of the cat. J Anat 98:611–630.

Moriizumi T, Hattori T. 1992. Ultrastructural morphology of projections from the medial geniculate nucleus and its adjacent region to the basal ganglia. Brain Res Bull 29:193–198.

Niimi K, Matsuoka H. 1979. Thalamocortical organization of the auditory system in the cat studied by retrograde axonal transport of horseradish peroxidase. Adv Anat Embryol Cell Biol 57:1–56.

Ottersen OP, Ben-Ari Y. 1979. Afferent connections to the amygdaloid complex of the rat and cat. I. Projections from the thalamus. J Comp Neurol 187:401–424.

Pape HC, McCormick DA. 1995. Electrophysiological and pharmacological properties of interneurons in the cat dorsal lateral geniculate nucleus. Neuroscience 68:1105–1125.

Paxino G, Watson C. 1986. The rat brain in stereotaxic coordinates. London: Academic Press.

Peschanski M. 1984. Trigeminal afferents to the diencephalon in the rat. Neuroscience 12:465–487.

Peruzzi D, Bartlett E, Smith PH, Oliver DL. 1997. A monosynaptic GABAergic input from the inferior colliculus to the medial geniculate body in the rat. J Neurosci 17:3766–3777.

Plourde G. 1996. The effects of propofol on the 40-Hz auditory steady-state response and on the electroencephalogram in humans. Anesth Analg 82:1015–1022.

Quirk GJ, Repa C, LeDoux JE. 1995. Fear conditioning enhances short-latency auditory responses of lateral amygdala neurons: parallel recordings in the freely behaving rat. Neuron 15:1029–1039.

Reinagel P, Godwin D, Sherman SM, Koch C. 1999. Encoding of visual information by LGN bursts. J Neurophysiol 81:2558–2569.

Rogan MT, LeDoux JE. 1995. LTP is accompanied by commensurate enhancement of auditory-evoked responses in a fear conditioning circuit. Neuron 15:127–136.

Roger M, Arnault P. 1989. Anatomical study of the connections of the primary auditory area in the rat. J Comp Neurol 287:339–356.

Ryugo DK, Weinberger NM. 1978. Differential plasticity of morphologically distinct neuron populations in the medical geniculate body of the cat during classical conditioning. Behav Biol 22:275–301.

Sailer CA, Hu H, Kaufmann WA, Trieb M, Schwarzer C, Storm JF, Knaus HG. 2002. Regional differences in distribution and functional expres-

sion of small-conductance Ca^{2+}-activated K^+ channels in rat brain. J Neurosci 22:9698–9707.

Scheel M. 1988. Topographic organization of the auditory thalamocortical system in the albino rat. Anat Embryol 179:181–190.

Scheibel ME, Scheibel AB. 1967. Structural organization of nonspecific thalamic nuclei and their projection toward cortex. Brain Res 6:60–94.

Senatorov VV, Hu B. 2002. Extracortical descending projections to the rat inferior colliculus. Neuroscience 115:243–250.

Shammah-Lagnado SJ, Alheid GF, Heimer L. 1996. Efferent connections of the caudal part of the globus pallidus in the rat. J Comp Neurol 376:489–507.

Sherman SM. 2001. Tonic and burst firing: dual modes of thalamocortical relay. Trends Neurosci. 24:122–126.

Sherman SM, Guillery RW. 2001. Exploring the thalamus. London: Academic Press.

Smith Y, Raju DV, Pare JF, Sidibe M. 2004. The thalamostriatal system: a highly specific network of the basal ganglia circuitry. Trends Neurosci 27:520–527.

Steriade M, McCormick DA, Sejnowski TJ. 1993. Thalamocortical oscillations in the sleeping and aroused brain. Science 262:679–685.

Swadlow HA, Gusev AG. 2001. The impact of "bursting" thalamic impulses at a neocortical synapse. Nat Neurosci 4:402–408.

Sukov W, Barth DS. 2001. Cellular mechanisms of thalamically evoked gamma oscillations in auditory cortex. J Neurophysiol 85:1235–1245.

Tennigkeit F, Puil E, Schwarz DW. 1997. Firing modes and membrane properties in lemniscal auditory thalamus. Acta Otolaryngol 117:254–257.

Van der Werf YD, Witter MP, Groenewegen HJ. 2002. The intralaminar and midline nuclei of the thalamus. Anatomical and functional evidence for participation in processes of arousal and awareness. Brain Res Brain Res Rev 39:107–140.

Vercelli A, Marini G, Tredici G. 2003. Anatomical organization of the telencephalic connections of the parafascicular nucleus in adult and developing rats. Eur J Neurosci 18:275–289.

Weinberger NM. 1998. Physiological memory in primary auditory cortex: characteristics and mechanisms. Neurobiol Learn Mem 70:226–251.

Weinberger NM, Javid R, Lepan B. 1995. Heterosynaptic long-term facilitation of sensory-evoked responses in the auditory cortex by stimulation of the magnocellular medial geniculate body in guinea pigs. Behav Neurosci 109:10–17.

Weyand TG, Boudreaux M, Guido W. 2001. Burst and tonic response modes in thalamic neurons during sleep and wakefulness. J Neurophysiol 85:1107–1118.

Winer JA, Larue DT. 1987. Patterns of reciprocity in auditory thalamocortical and corticothalamic connections: study with horseradish peroxidase and autoradiographic methods in the rat medial geniculate body. J Comp Neurol 257:282–315.

Winer JA, Larue DT. 1988. Anatomy of glutamic acid decarboxylase immunoreactive neurons and axons in the rat medial geniculate body. J Comp Neurol 278:47–68.

Winer JA, Morest DK. 1983. The medial division of the medial geniculate body of the cat: implications for thalamic organization. J Neurosci 3:2629–2651.

Winer JA, Kelly JB, Larue DT. 1999. Neural architecture of the rat medial geniculate body. Hearing Res 130:19–41.

Winer JA, Chernock ML, Larue DT, Cheung SW. 2002. Descending projections to the inferior colliculus from the posterior thalamus and the auditory cortex in rat, cat, and monkey. Hearing Res 168:181–195.

Ying SW, Goldstein PA. 2005. Propofol-block of SK channels in reticular thalamic neurons enhances GABAergic inhibition in relay neurons. J. Neurophysiol 93:1935–1948.

Yu YQ, Xiong Y, Chan YS, He J. 2004. In vivo intracellular responses of the medial geniculate neurones to acoustic stimuli in anaesthetized guinea pigs. J Physiol 560:191–205.